DISCRETE AND CONTINUOUS
DYNAMICAL SYSTEMS
Volume **18**, Number **2&3**, June & July **2007**

Website: http://AIMsciences.org

pp. **221–251**

DYNAMICS OF A PREDATOR-PREY MODEL WITH NON-MONOTONIC RESPONSE FUNCTION

H.W. Broer

Department of Mathematics, University of Groningen
P.O. Box 800, 9700 AV Groningen, the Netherlands

K. Saleh

Department of Mathematics, University of Groningen
P.O. Box 800, 9700 AV Groningen, the Netherlands

V. Naudot

Mathematics Institute
University of Warwick, Coventry CV4 7AL, UK

R. Roussarie

Institut Mathématiques de Bourgogne
CNRS, 9, avenue Alain Savary, B.P. 47 870, 21078 Dijon cedex, France

Abstract. A five-parameter family of planar vector fields, which models the dynamics of certain populations of predators and their prey, is discussed. The family is a variation of the classical Volterra-Lotka system by taking into account group defense strategy, competition between prey and competition between predators. Also we initiate computer-assisted research on time-periodic perturbations, which model seasonal dependence. We are interested in persistent features. For the planar autonomous model this amounts to structurally stable phase portraits. We focus on the attractors, where it turns out that multi-stability occurs. Further, the bifurcations between the various domains of structural stability are investigated. It is possible to fix the values of two of the parameters and study the bifurcations in terms of the remaining three. Here we find several codimension 3 bifurcations that form organizing centres for the global bifurcation set. Studying the time-periodic system, our main interest is the chaotic dynamics. We plot several numerical examples of strange attractors.

1. **Introduction.** This paper deals with a particular family of planar vector fields which models the dynamics of the populations of predators and their prey in a given ecosystem. This approach is a variation on the classical Volterra-Lotka predator-prey system [42,65]. The latter system has a first integral, implying that the populations of both prey and predators oscillate permanently given any generic positive initial values. For the Volterra-Lotka system the change of the prey density per unit of time per predator, called the *response function* [58], is proportional to the prey density. This means that there is no saturation of the predator when the amount of available prey is large. However, it is more realistic to consider a nonlinear and

2000 *Mathematics Subject Classification.* 58K45, 34C23, 34C60,37D15, 37D45.

Key words and phrases. Predator-prey dynamics, bifurcation, organizing centre and non-monotonic response function.

bounded response function. Different response functions have been used to model the predator response, see for instance [33, 39, 54].

Recently, Zhu et al. [68] studied the following predator-prey model

$$\begin{cases} \dot{x} &= x(a-\lambda x) - yP(x) \qquad \text{(prey)}, \\ \dot{y} &= -\delta y + yQ(x) \qquad \text{(predator)}. \end{cases} \tag{1}$$

The variables x and y denote the density of the prey and predator populations respectively, while $P(x)$ is a non-monotonic response function [2] given by

$$P(x) = \frac{mx}{\alpha x^2 + \beta x + 1}, \tag{2}$$

where α, m are nonnegative and where $\beta > -2\sqrt{\alpha}$. Note that $\alpha = 0$ gives a particular response function, which is used in [5, 39, 52].

In the absence of predators, the prey has logistic growth. The coefficient a represents the intrinsic growth rate of the prey, while $\lambda > 0$ is the rate of competition or resource limitation of prey. The natural death rate of the predator is given by $\delta > 0$. In Gause's model [34] the function $Q(x)$ is given by $Q(x) = cP(x)$, where $c > 0$ is the rate of conversion between prey and predator.

Several experiments by Andrew [2], Boon and Landelout [7] and by Edwards [31] indicate that non-monotonic responses are present at the microbial level when the nutrient (prey) concentration reaches a high level, in which case an inhibitory effect on the specific growth rate occurs. Another earlier example of this phenomenon is observed by Tener [62]. Indeed, lone prey (musk ox) can be successfully attacked by predators (wolves). However, small herds of musk oxen (2 to 6 animals) are attacked with less success. Furthermore, no successful attack has been observed in large herds. For more examples of populations that use the group defense strategy, see [33, 54]. Also compare [4] in which a predator-prey model is considered with herbivores as predators and plants as prey: the number of herbivores decreases when the density of plants become particularly dense.

1.1. **Setting of the problem.** In this paper, we study the following family

$$\begin{cases} \dot{x} &= x(1-\lambda x) - \dfrac{xy}{\alpha x^2 + \beta x + 1} \qquad \text{(prey)}, \\ \dot{y} &= y(-\delta - \mu y) + \dfrac{xy}{\alpha x^2 + \beta x + 1} \qquad \text{(predator)}, \end{cases} \tag{3}$$

where $\alpha \geq 0$, $\delta > 0$, $\lambda > 0$, $\mu \geq 0$ and $\beta > -2\sqrt{\alpha}$ are parameters. We note that (3) is obtained from (1) by adding the term $-\mu y^2$ to the second equation and after scaling x and y, as well as the parameters and the time t. In this way we take into account predators competition for resources other than prey, see [5, 6]. The non-negative coefficient μ is the rate of competition amongst predators.

Our goal is to understand the structurally stable dynamics of system (3) and in particular the attractors with their basins where we have a special interest for multi-stability. Meanwhile we present a quite general method of analyzing such a system. Here the mathematical background of the specific case study is fully developed, and a clear distinction is made between proven and numerical results.

By surgery [44, 47] the structurally stable phase portraits of system (3) are reduced to new ones without limit cycles. Index theory and the Poincaré-Bendixon Theorem [44, 48] are applied to get a complete classification of the reduced (phase) portraits, see Figure 2. The latter portraits serve to predict bifurcations occurring in the family, which help to understand the dynamics of system (3) and discover all

possible phase portraits. Here the occurrence of periodic orbits can be predicted and checked numerically. Moreover, we apply advanced bifurcation theory to explain the dynamics of the system.

Besides Zhu's model (1), Bazykin's model [5] occurs as a special case of system (3), namely by setting $\alpha = 0$. This means that Bazykin does not consider group defence in the prey population. The bifurcation sets of both models contain certain degenerate version of Bogdanov-Takens bifurcations [28,29] which act as organizing centres. In the present paper both α and μ are considered to be non-negative. This means that both group defense strategy in the prey population and competition amongst predators are taken into account. We recover the codimension 3 bifurcations that have been found in Bazykin's and Zhu's models. Moreover, we also find degenerate versions of transcritical bifurcation [37,41] that form organizing centres of the global bifurcation set. The latter investigations were lacking in [5,68].

We also address the modification of system (3), where a small parametric forcing is applied in the parameter λ, as suggested by Rinaldi et al. [52]

$$\lambda = \lambda_0 \left(1 + \varepsilon \sin\left(\frac{2\pi}{\omega} t\right)\right), \tag{4}$$

where $\varepsilon < 1$ is a perturbation parameter and ω is a constant. We are interested in 'large scale' strange attractors.

Remarks. We indicate a few further variations on the above approach.

1. In addition to (4), one sets

$$a = a_0 \left(1 + \varepsilon \sin\left(\frac{2\pi}{\omega} t\right)\right),$$

   which expresses seasonal growth rate fluctuation, see for instance [52].
2. Another choice [32,67] of non-monotonic response function is given by

$$P(x) = \gamma_1 x e^{-\gamma_2 x},\ 0 < \gamma_1,\ 0 \leq \gamma_2. \tag{5}$$

   which is briefly discussed in §2.1.

1.2. **Outline.** This paper is organized as follows. In §2 we describe the approach of our research, formulating the main results of the investigation. In §3 we give a topological classification of the possible Reduced Morse-Smale portraits of system (3). In §4 we perform a bifurcation analysis of system (3), applying a standard normal form procedure. Numerically, we detect homoclinic loops and saddle-node bifurcations of limit cycles. In §5 we give a few biological interpretations of the results. Also several related models are discussed as these appear in the literature, indicating possible relationships with the present approach.

2. Strategy of research and statement of results.

In this section we describe the methodology of the research and give the main results of this paper.

2.1. **Strategy of research.** We first sketch the approach of the present investigation.

Trapping domains and Reduced Morse-Smale portraits. Our study concerns the dynamics of (3) in the closed first quadrant clos($\mathcal{Q}$) where $\mathcal{Q} = \{(x, y) \in \mathbb{R}^2 | x > 0,\ y > 0\}$ with boundary $\partial\mathcal{Q}$, which are both invariant under the flow. We shall show that system (3) has a compact *trapping domain* $\mathcal{B}_p \subset$ clos($\mathcal{Q}$): all orbits in clos($\mathcal{Q}$) enter $\mathcal{B}_p$ after finite time and do not leave it again, see Figure 1-(a). For the moment we restrict the attention to structurally stable (or Morse-Smale) dynamics. In the interior of $\mathcal{B}_p$, there can be at most two stable equilibria and possibly one saddle-point. We study these singular points using algebraic tools, occasionally supported by computer algebra. Also we numerically detect several cases with one or two limit cycles. Here we often use numerical continuation, where the algebraic detection of Hopf or Bogdanov-Takens bifurcations helps to initiate the continuation process.

As mentioned in §1 our approach is to reduce, by surgery, the structurally stable phase portraits to new portraits without limit cycles. During surgery we change a part of the phase space by smooth cutting and pasting [44, 47]. Next with the help of topological means (Poincaré-Hopf Index Theorem, Poincaré-Bendixson Theorem [44, 48]) we find a complete classification of the reduced portraits. Compare with Figure 2 and see §2.2, in particular Theorem 1 as well as its proof in §3 for more details.

The description of all possible reduced portraits gives an idea of bifurcations occurring in the original family (3). For instance, when looking at Figure 2 we expect the presence of a homoclinic bifurcation: exchanging a saddle-sink pair [a-2] with a saddle-source pair [a-3]. Since we have saddle-node (transition from [a-1] to [a-2] in Figure 2) and homoclinic bifurcations, one may expect the existence of a Bogdanov-Takens bifurcation and even the presence of a singularity of nilpotent-focus type NF_3.

We note that the reduced portraits are classified by only considering topological aspects of the family. Therefore, this idea can also be applied to other planar systems with a compact trapping domain. In this sense the present paper gives a method to study similar systems.

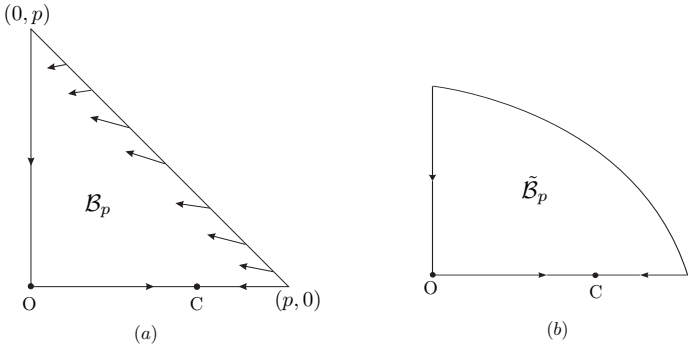

FIGURE 1. (a): Compact trapping domain $\mathcal{B}_p$ found with a Lyapunov function, see §2. The point C is a singularity on the x-axis. (b): A narrower trapping domain $\tilde{\mathcal{B}}_p \subset \mathcal{B}_p$ found numerically with help of Matlab [38] and Matcont [36].

Organization of the parameter space. Our main interest is the dense-open subset of the five-dimensional parameter space with structurally stable dynamics. The

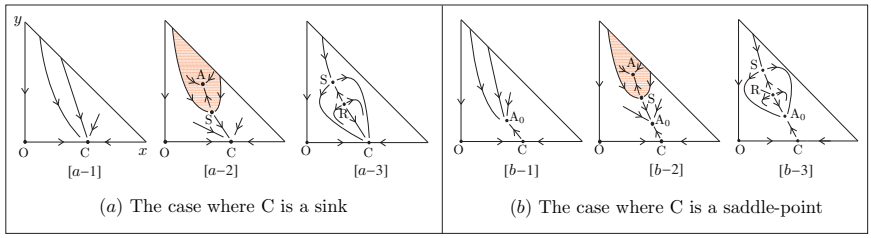

FIGURE 2. Reduced Morse-Smale portraits occurring in system (3); A is a sink (the corresponding basin is dashed), S is a saddle-point and R a source. (a): The case where C is a sink (with corresponding basin in white). (b): The case where C is a saddle-point. In the latter case the interior of the trapping domain always contains an attractor denoted by A_0 with basin in white. Bi-stability only occurs in portraits [a-2] and [b-2].

complement of this set is the bifurcation set, which contains strata of different codimension.

It turns out that the parameters δ and λ play a minor role and that we can describe the bifurcation set as follows. Let $\Delta = \{(\delta, \lambda) \in \mathbb{R}^2 | \delta > 0, \lambda > 0\}$ and $\mathcal{W} = \{(\alpha, \beta, \mu) \in \mathbb{R}^3 | \alpha \geq 0, \beta > -2\sqrt{\alpha}, \mu \geq 0\}$. We fix $(\delta, \lambda) \in \Delta$ and the bifurcation of (3) is described in the space $\mathcal{W}$. To discuss this we introduce the projection

$$\Pi : \mathcal{W} \times \Delta \to \Delta, \, (\alpha, \beta, \mu, \delta, \lambda) \mapsto (\delta, \lambda),$$

studying all the fibers $\Pi^{-1}(\delta, \lambda)$. This argument works as long as the fibers are transversal to the bifurcation set consisting of singularities of nilpotent-focus type (NF_3), in which case we only have to consider bifurcations of codimension less than or equal to 3. It turns out that this is the case in the complement of a smooth curve $\mathcal{C}$, compare with Figure 3-(a), see §2.2 as well as §4.4 for details. Indeed, as stated in Theorem 2, the bifurcation set in $\mathcal{W}$ is qualitatively constant above each open region Δ_1 and Δ_2, separated by $\mathcal{C}$. Above the curve $\mathcal{C}$ there is a folding of the bifurcation set at which the fiber $\Pi^{-1}(\delta, \lambda)$ is tangent to it. Also certain bifurcations of codimension 4 or 5 occur in $\Delta \times \mathcal{W}$ but only concern values of (x, y) outside $\mathcal{Q}$ and we do not pay further attention to these.

When restricting to Δ_1 and Δ_2 the codimension 3 bifurcations inside $\mathcal{W}$ act as organizing centres. This means that when taking two-dimensional sections in $\mathcal{W}$ we see a semi-global picture organized by the trace of the codimension 3 bifurcations.

For each region Δ_1 and Δ_2 the associated bifurcation set in $\mathcal{W}$ is depicted in Figure 3-(b) and Figure 3-(c), respectively. Figure 3-(c) shows that the bifurcation set possesses several codimension 2 curves subordinate to four codimension 3 points which act as organizing centres. Now we explain how to understand the bifurcations up to codimension 1.

Organizing centres and two-dimensional bifurcation diagrams. Given the organizing centres of the bifurcation sets in $\mathcal{W}$, we take two-dimensional sections $\mathcal{S}_i$, $i = 1, \ldots, 6$, transversal to the codimension 2 curves as indicated in Figure 3. Each two-dimensional section intersects codimension 0 strata in several open regions separated by codimension 1 curves. The associated two-dimensional bifurcation diagrams will be shown, emphasizing the basins of attraction and the possible multi-stability. In the diagrams, we use the narrower trapping domains obtained

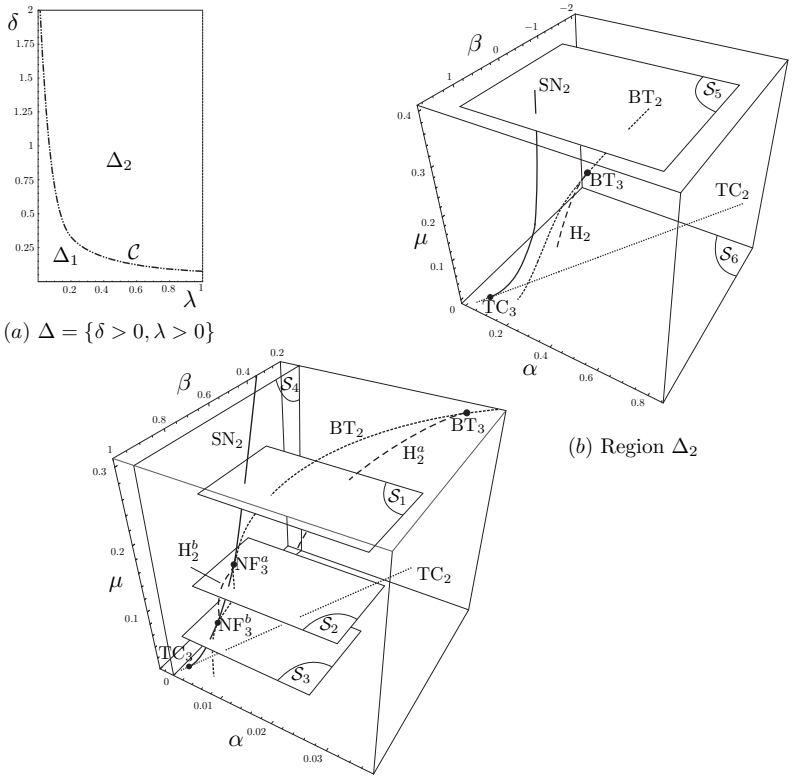

(a) $\Delta = \{\delta > 0, \lambda > 0\}$

(b) Region Δ_2

(c) Region Δ_1

FIGURE 3. (a): Region $\Delta = \{\delta > 0, \lambda > 0\}$. ($b$): Bifurcation set in $\mathcal{W} = \{\alpha \geq 0, \beta > -2\sqrt{\alpha}, \mu \geq 0\}$ when $(\delta, \lambda) \in \Delta_2$. Section $\mathcal{S}_6 = \{\mu = 0\}$ is the two-dimensional section associated to the bifurcation diagram of Zhu's model [68]. (c): Similar to (b) for the case $(\delta, \lambda) \in \Delta_1$. Section $\mathcal{S}_4 = \{\mu = 0\}$ covers the case of Bazykin's model [41]. For terminology see Table 1.

numerically with help of Matlab [38] and Matcont [36], see Figure 1-(b). Furthermore, for each corresponding two-dimensional bifurcation diagram, the *Reduced Morse-Smale* (*bifurcation*) *diagram* is given.

We illustrate our strategy in Figure 4-(a) by presenting one of the two-dimensional bifurcation diagrams (in $\mathcal{S}_1$), for the terminology referring to Table 1. From Figure 4-(a) the corresponding Reduced Morse-Smale diagram is obtained by removing the Hopf curve, see Figure 7-(a).

Limit cycles and homoclinic loops. We describe how limit cycles can come into existence by codimension 1 bifurcations. Limit cycles may be created by Hopf bifurcation (H_1) (see for instance regions 1 and 7 in Figure 4-(a)), by saddle-node bifurcation of limit cycles ($SNLC_1$) (see regions 9 and 11 in the same Figure 4-(a)) and by homoclinic bifurcation (L_1) (or Blue Sky catatrophe [1], see regions 1 and 12 in Figure 4-(a)). The occurrence of limit cycles is investigated numerically (continuation) with help of Matlab [38], Matcont [36] and Auto2000 [27].

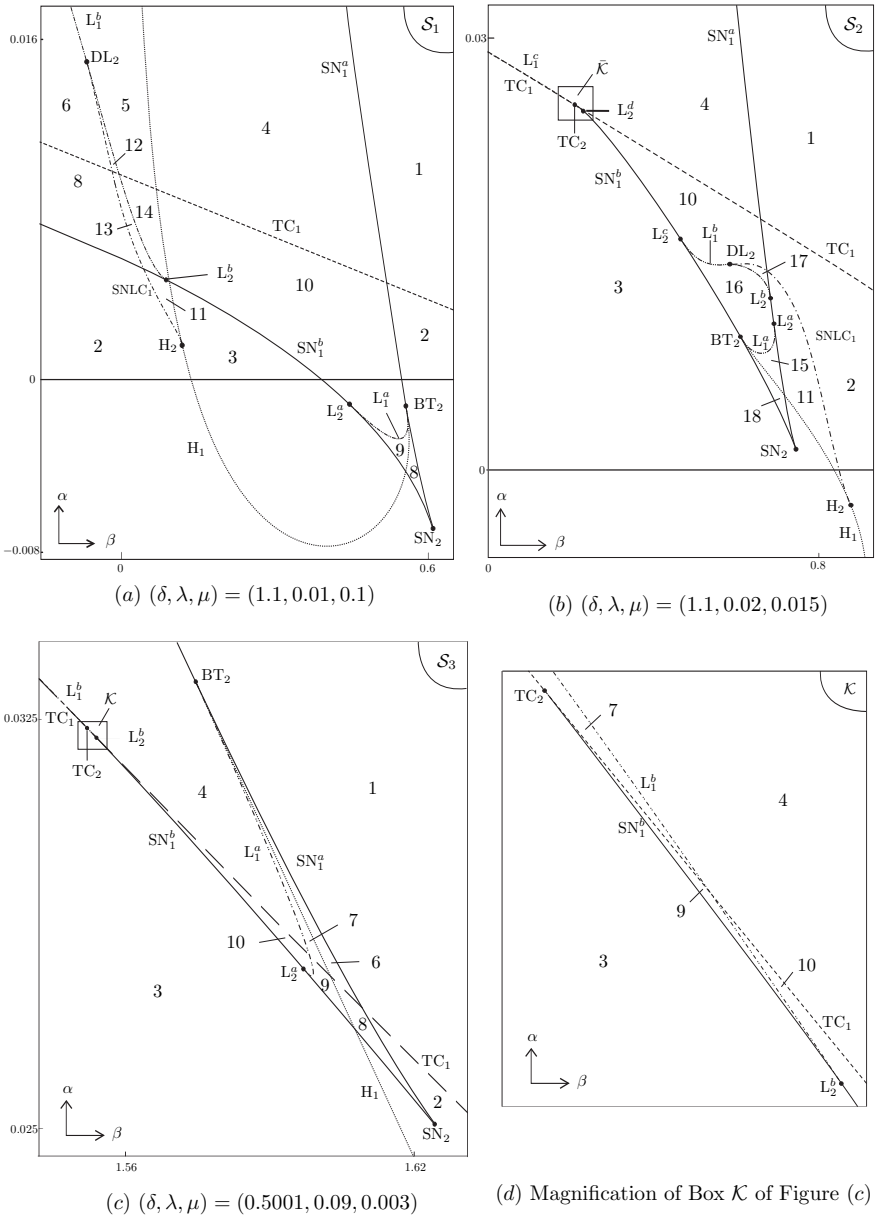

(*a*) $(\delta, \lambda, \mu) = (1.1, 0.01, 0.1)$

(*b*) $(\delta, \lambda, \mu) = (1.1, 0.02, 0.015)$

(*c*) $(\delta, \lambda, \mu) = (0.5001, 0.09, 0.003)$

(*d*) Magnification of Box $\mathcal{K}$ of Figure (*c*)

FIGURE 4. Two-dimensional bifurcation diagrams of system (3) associated to sections $\mathcal{S}_1$, $\mathcal{S}_2$ and $\mathcal{S}_3$ indicated in Figure 3. Bifurcation diagram in box $\bar{\mathcal{K}}$ is topologically equivalent to that in box $\mathcal{K}$. Phase portrait for every region is given in Figure 6. For terminology see Table 1.

In principle limit cycles also could be created by heteroclinic connections, but in our case this does not apply, since there can be at most one saddle-point in the interior of the trapping domain (see Theorem 1).

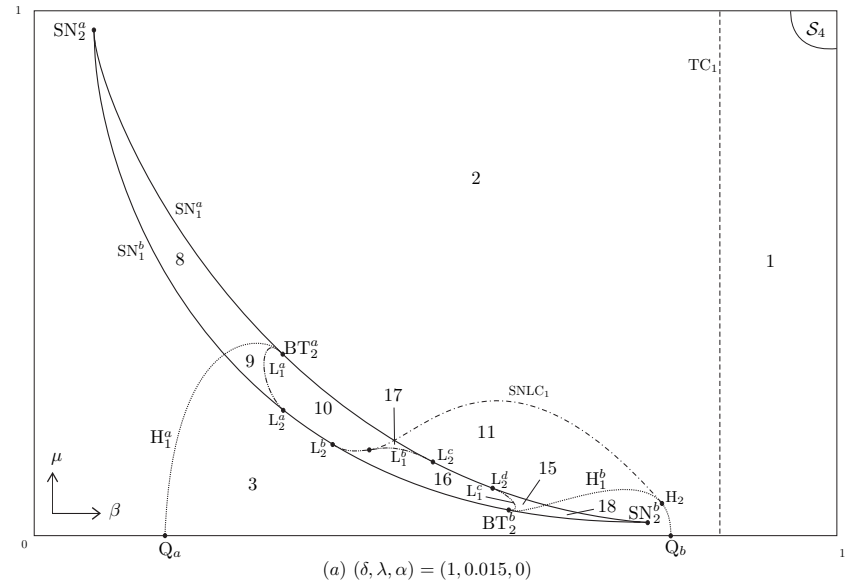

(a) $(\delta, \lambda, \alpha) = (1, 0.015, 0)$

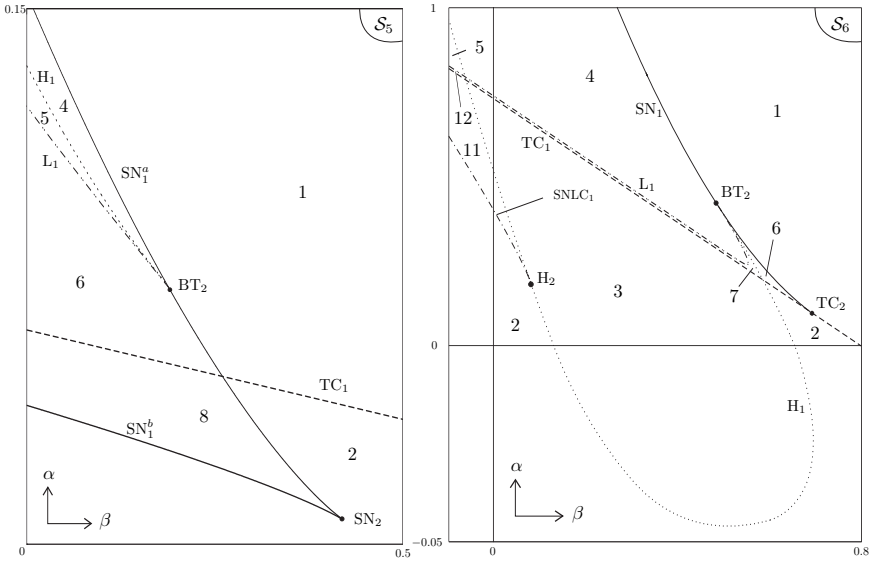

(b) $(\delta, \lambda, \mu) = (0.8, 0.05, 0.3)$ (c) $(\delta, \lambda, \mu) = (1.1, 0.1, 0)$

FIGURE 5. Two-dimensional bifurcation diagrams of system (3) associated to sections $\mathcal{S}_4$, $\mathcal{S}_5$ and $\mathcal{S}_6$ indicated in Figure 3. Phase portrait for every region is given in Figure 6. For terminology see Table 1.

As said before, all local bifurcations can be detected algebraically, which is not the case for the global bifurcations L_1 and $SNLC_1$. Again we resort to numerical continuation methods, using various codimension 2 bifurcations to create initial data. For example, in Figure 4-(a), the degenerate Hopf bifurcation H_2 'generates'

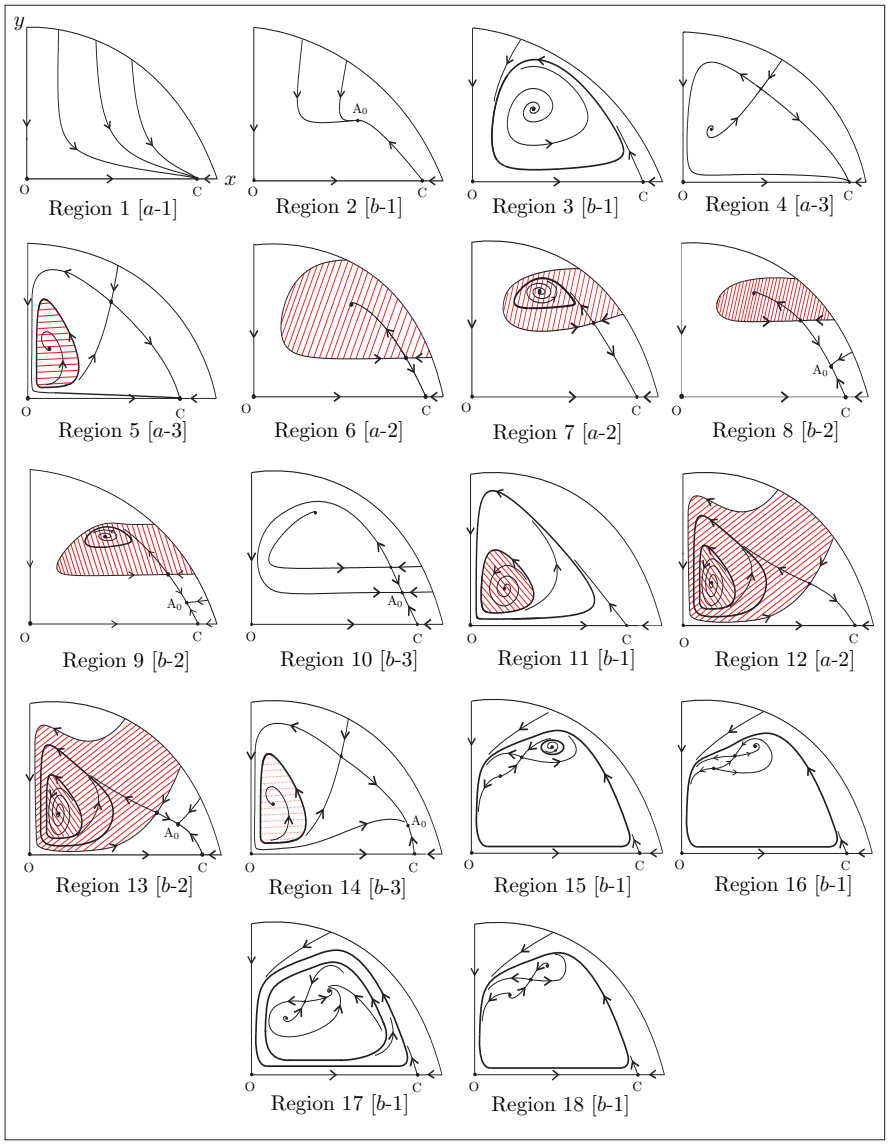

FIGURE 6. Generic phase portraits of system (3) referring to the corresponding Reduced Morse-Smale portraits of Figure 2. Bi-stability in regions 8 and 9 both correspond to [b-2] in Figure 2. Bi-stability also holds in region 11 (corresponding to [b-1], which does not show bi-stability). The white basin of attraction is either for C or for A_0, while the shaded ones are for other attractors.

the curve $SNLC_1$, while the Bogdanov-Takens bifurcation BT_2 generates the curve L_1^a. More details are given in §4.4.

Parametric forcing. Dynamical properties of system (3) with parametric forcing (4) can be expressed in terms of the stroboscopic map

$$\mathcal{P}_\varepsilon : \mathbb{R}^2 \to \mathbb{R}^2, \ (x, y) \mapsto \varphi_\varepsilon^1(x, y), \tag{6}$$

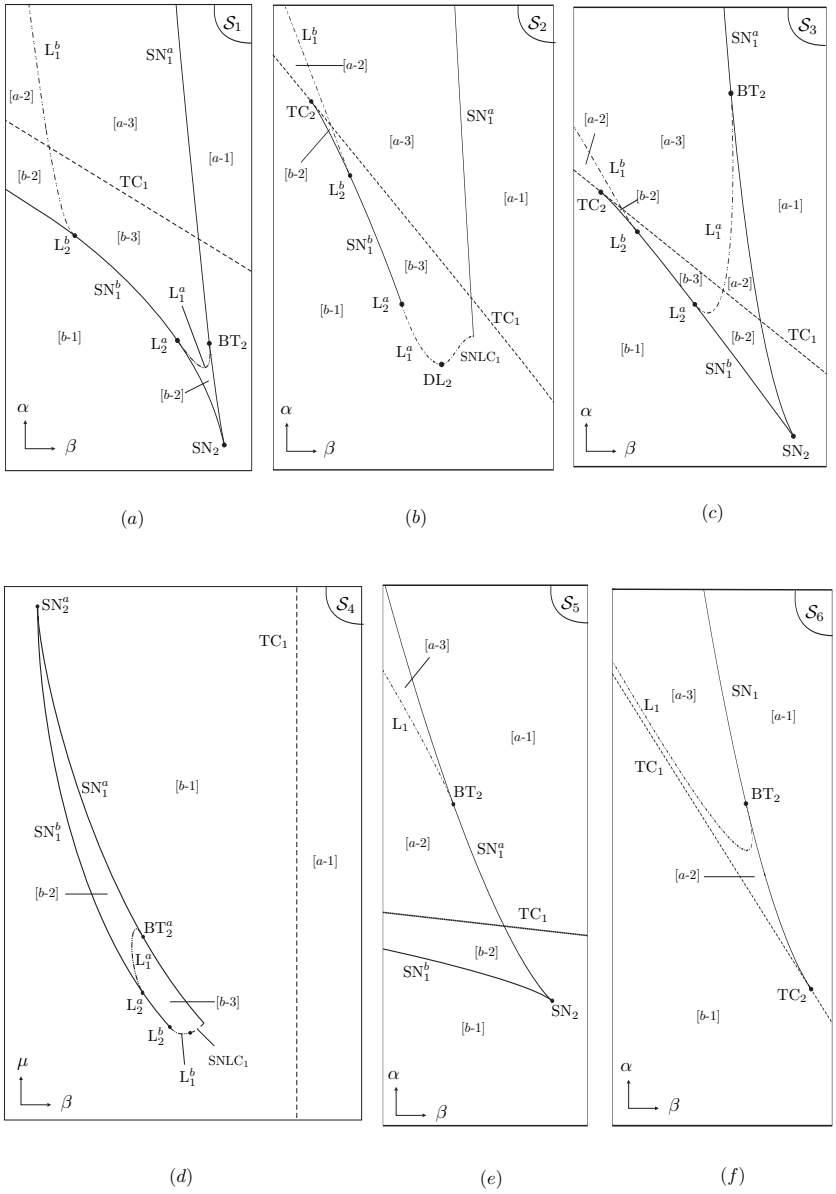

FIGURE 7. Reduced Morse-Smale diagrams obtained from Figures 4 and 5. Generic phase portraits are given in Figure 2. For terminology see Table 1.

where φ_ε^t denotes the flow of the time-periodic system written as a three-dimensional vector field $X_\varepsilon = X_\varepsilon(x, y, t; \alpha, \beta, \mu, \delta, \lambda)$. Fixed points of $\mathcal{P}_\varepsilon$ correspond to periodic solutions of X_ε with period ω, and similarly invariant circles to invariant 2-tori.

We take $|\varepsilon|$ small, so that X_ε is a perturbation of the autonomous system X_0 given in (3). As an example, we plot a few attractors for $\mathcal{P}_\varepsilon$ in Figures 8, 9 and 10, for parameter values near the homoclinic curve L_1^a in region 9 of Figure 4-(a). We have numerical evidence for the following statements. Figure 8 shows a

Notation	Name	Incidence
TC_1	Transcritical	
TC_2	Degenerate transcritical	$SN_1 + TC_1$
TC_3	Doubly degenerate transcritical	$SN_2 + TC_2$
SN_1	Saddle-node	
SN_2	Cusp	$SN_1 + SN_1$
BT_2	Bogdanov-Takens	$SN_1 + H_1 + L_1$
BT_3	Degenerate Bogdanov-Takens	$BT_2 + H_2 + DL_2$
NF_3	Singularity of nilpotent-focus type	$SN_2 + BT_2 + L_2 + H_2$
H_1	Hopf	
H_2	Degenerate Hopf	$H_1 + SNLC_1$
L_1	Homoclinic (or Blue Sky)	
L_2	Homoclinic at saddle-node	$L_1 + SN_1$
DL_2	Degenerate homoclinic	$L_1 + SNLC_1$
$SNLC_1$	Saddle-node of limit cycles	

TABLE 1. List of bifurcations occurring in system (3). This notation will be kept throughout. All bifurcations are local except the latter four, which are global. In all cases the subscript indicates the codimension of the bifurcation. In the column 'Incidence' we put the subordinate bifurcations of highest codimension. See [1, 28, 29, 37, 41] for details concerning the terminology and fine structure.

strange attractor that consists of 11 connected components mapped by $\mathcal{P}_\varepsilon$ to one another in a cyclic way. These components globalize in Figure 9 in a scenario called heteroclinic tangency (or boundary crisis), compare [19]. Figure 10 shows an invariant C^0-circle, associated to region 9 in Figure 4-(a) when we approach the codimension 2 homoclinic point L_2^b.

The present approach also applies to system (3) with the exponential response function (5). We depict a strange attractor in Figure 11.

2.2. **Statement of the results.** We formulate the main results of this paper in a more precise way. Also an overview of two-dimensional bifurcation diagrams is presented with descriptions of the role of the organizing centres and with the corresponding Reduced Morse-Smale diagrams. A brief discussion is included on the behaviour of the stroboscopic map (6), based on perturbation theory.

The bifurcation sets and the associated phase portraits are drawn with the help of Mathematica [66], Matlab [38], Auto2000 [27] and Matcont [36].

Results. The first theorem treats general properties of system (3) with response function (2). It contains a classification of the structurally stable case, which covers a dense-open subset of the parameter space $\Delta \times \mathcal{W}$. As explained later (§3.1), for planar vector fields structural stability is completely characterized by the Morse-Smale properties. To each Morse-Smale vector field we associate a Reduced Morse-Smale vector field without limit cycles, where both concepts coincide when there are no limit cycles with which to start. Recall that we only consider the closed first quadrant $\mathrm{clos}(\mathcal{Q})$ of the (x, y)-plane.

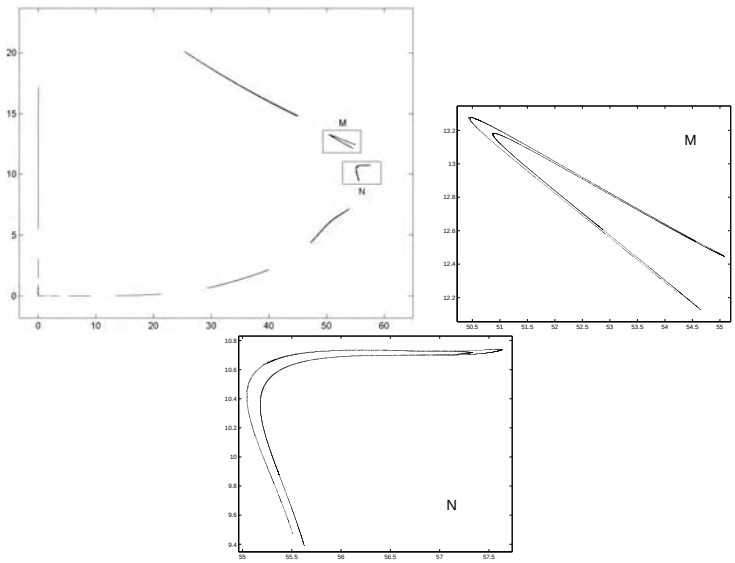

FIGURE 8. Left: Strange attractor for $\mathcal{P}_\varepsilon$ for parameter values in region 9 of Figure 4-(a) using 500 000 iterations, $(\alpha, \beta, \delta, \mu, \lambda) = (0.007, 0.036, 1.01, 0.1, 0.01)$, $\varepsilon = 0.6$ and $\omega = 1$. The attractor consists of 11 connected components mapped by P_ε to one another in a cyclic way. Middle: Magnification of box M in the figure on the top. Right: Magnification of box N of the figure on the top.

Theorem 1. (GENERAL PROPERTIES) *System* (*3*) *with response function* (*2*) *has the following properties:*

1. (TRAPPING DOMAIN) *The domain* $\mathcal{B}_p = \{(x, y) \mid 0 \le x,\ 0 \le y,\ x+y \le p\}$ *with* $p > 1/\lambda((1-\delta)^2/(4\delta)+1)$, *is a trapping domain, meaning that it is invariant for positive time evolution and also captures all integral curves starting in* $\mathrm{clos}(\mathcal{Q})$.
2. (NUMBER OF SINGULARITIES) *There are two singularities on the boundary* $\partial\mathcal{Q}$, *namely* $(0,0)$ *which is a hyperbolic saddle-point and* $\mathrm{C}_\lambda = (1/\lambda, 0)$, *which is* (*semi-*) *hyperbolic with* $\{x > 0, y = 0\} \subset W^s(\mathrm{C}_\lambda)$. *In* $\mathcal{Q}$ *there can be no more than three singularities and the cases with zero, one, two and three singularities all occur.*
3. (CLASSIFICATION OF THE REDUCED MORSE-SMALE CASE) *Exactly six topological types of Reduced Morse-Smale vector fields occur, listed in Figure 2.*

For a proof see §3.

In what follows we refer to [28, 29, 37, 41] for details concerning the codimension 3 bifurcation points. The following theorem is illustrated by Figure 3.

Theorem 2. (ORGANIZING CENTRES) *Consider system* (*3*) *with response function* (*2*). *In the parameter space* $\mathbb{R}^5 = \{\alpha, \beta, \mu, \delta, \lambda\}$ *consider the projection* $\Pi : \Delta \times \mathcal{W} \to \Delta$, *where* $\Delta = \{0 < \delta, 0 < \lambda\}$ *and* $\mathcal{W} = \{\alpha \ge 0, \beta > -2\sqrt{\alpha}, \mu \ge 0\}$. *There exists a smooth curve* $\mathcal{C}$ *that separates* Δ *into two open regions* Δ_1 *and* Δ_2.

For all $(\delta, \lambda) \in \Delta_1$ *the corresponding* 3*-dimensional bifurcation set in* $\mathcal{W}$ *has four organizing centres of codimension* 3 :

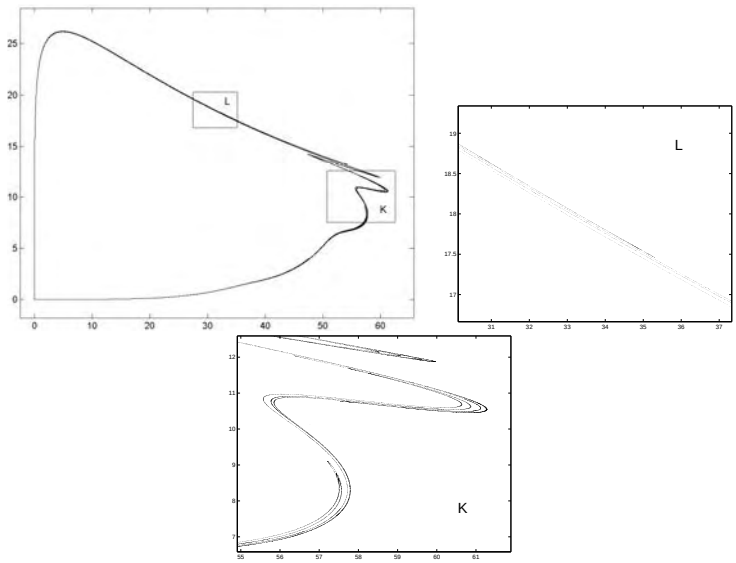

FIGURE 9. Left: Viana-like strange attractor for $\mathcal{P}_\varepsilon$ for parameter values in region 9 of Figure 4-(a) using 500 000 iterations, $(\alpha, \beta, \delta, \mu, \lambda) = (0.007, 0.036, 1.01, 0.1, 0.01)$, $\varepsilon = 0.99$ and $\omega = 1$, compare [19]. Middle: Magnification of box L in the figure on the top. Right: Magnification of box K in the figure on the top.

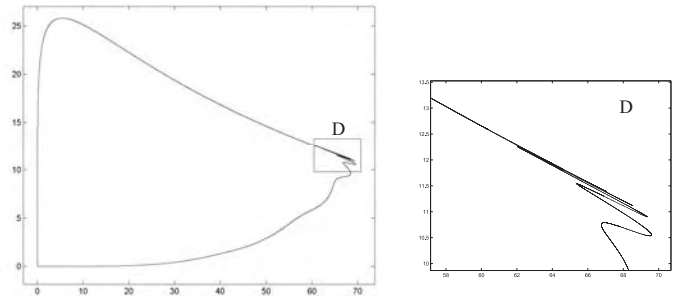

FIGURE 10. Left: C^0 circle for $\mathcal{P}_\varepsilon$ for parameter values in region 9 of Figure 4-(a) using 500 000 iterations, $(\alpha, \beta, \delta, \mu, \lambda) = (0.0061, 0.06, 1.01, 0.1, 0.01)$, $\varepsilon = 0.7$ and $\omega = 1$. Right: Magnification of box D in the figure on the left.

1. *One transcritical point* (TC_3),
2. *Two nilpotent-focus type points* (NF_3^a *and* NF_3^b) *connected by a smooth degenerate Hopf curve* (H_2) *and by a smooth cusp curve* (SN_2) *containing* TC_3,
3. *One Bogdanov-Takens point* (BT_3) *connected to* NF_3^b *by a smooth Bogdanov-Takens curve* (BT_2).

Furthermore, the points NF_3^a, NF_3^b *collide when* (δ, λ) *approach* $\mathcal{C}$ *and disappear for* $(\delta, \lambda) \in \Delta_2$. *The organizing centers* TC_3 *and* BT_3 *remain.*

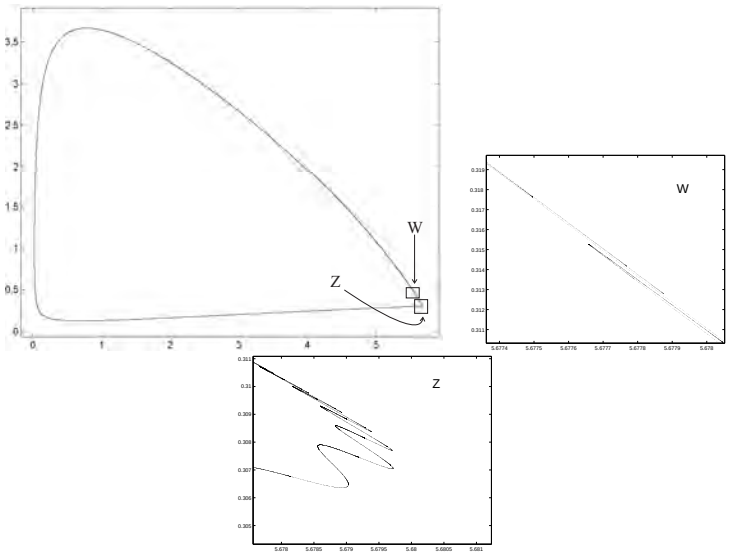

FIGURE 11. Left: Strange attractor for $\mathcal{P}_\varepsilon$ of system (3) with response function (5) and forcing (4) using 500 000 iterations, $(\delta, \mu, \lambda, \gamma_1, \gamma_2) = (0.5, 0.01, 0.241, 0.5, 1)$, $\varepsilon = 0.9$ and $\omega = 1$. Middle: Magnification of box W in the figure on the top. Right: Magnification of box Z of the figure on the top.

For a proof see §4. We refer to [17, 56] for details.

Remarks.

1. All bifurcations that occur in system (3) with response function (2), are known to have finite cyclicity, for definitions and details see [53]. From this it follows that in any compact region of the parameter space, such that the projection under Π is bounded away from the curve $\mathcal{C}$, there is a uniform bound on the number of limit cycles [53]. Although no theoretical information is known on this bound, numerically we find that in our case it is equal to 2.
2. From the above remark and Theorem 1 we can give a complete classification of all Morse-Smale types. Indeed, as will be shown in §3.4, this type is completely determined by the Reduced Morse-Smale type and the number and positions of these limit cycles.

Next we explain the role of the organizing centres and the actual realization of all Reduced Morse-Smale portraits of Figure 2.

Tour guide for the two-dimensional bifurcation diagrams. The illustrating example that concerns two-dimensional section $\mathcal{S}_1$ (Figure 4-(a)) is now generalized to all sections $\mathcal{S}_2$, $\mathcal{S}_3$, $\mathcal{S}_4$, $\mathcal{S}_5$ and $\mathcal{S}_6$ of Figure 3. The corresponding two-dimensional bifurcation diagrams are given in Figures 4 and 5. Furthermore, for each two-dimensional bifurcation diagram the Reduced Morse-Smale diagram is given. Compare with Figure 4-(a) with Reduced Morse-Smale diagram in Figure 7-(a). For instance, Figure 4-(c) plays the same role with Reduced Morse-Smale diagram shown in Figure 7-(c).

Each two-dimensional bifurcation diagram describes the dynamics in the corresponding connected component of the complement of the bifurcation set, where the

phase portraits are of Morse-Smale type. Transitions between these components are bifurcations. If one takes a generic path through parameter space, one meets just codimension 1 bifurcations, compare with Table 1. We mention the transcritical, the saddle-node and the Hopf bifurcation as local bifurcations, while the homoclinic bifurcation (or Blue Sky catastrophe) and the saddle-node bifurcation of limit cycles are global [10, 37, 41]. The bifurcations of codimension up to 3, serve as organizing centres that locally (and often semi-globally) determine the geometry of the bifurcation set.

All pictures are illustrations for appropriate parameter values. Other choices will give topologically equivalent pictures [28, 29]. As an example, consider Figure 4-(a) which illustrates two-dimensional bifurcation diagram in $\mathcal{S}_1$ of Figure 3-(b). Here we select $(\delta, \lambda) = (1.01, 0.01) \in \Delta_1$ and $\mu = 0.1$. Varying μ in the neighbourhood of $\mu = 0.1$ will give pictures similar to Figure 4-(a) as long as the associated two-dimensional section does not cross the points BT_3 and NF_3^a. Choosing other values of $(\delta, \lambda) \in \Delta_1$ and taking μ in such a way that the corresponding two-dimensional section is in between the points BT_3 and NF_3^a also will give topologically equivalent picture as in Figure 4-(a).

Recall that our investigation is in $\mathbb{R}^7 = \mathcal{W} \times \Delta \times \mathrm{clos}\mathcal{Q}$. As explained in §2.1, we do not have to pay attention to bifurcations of codimension higher than 3. All pictures are depicted with help of codimension 3 bifurcations which act as organizing centres. All subordinate bifurcations expected in [28, 29, 37, 41] occur.

The time-periodic system. As announced in §2.1, we here discuss the general relationship between the autonomous system X_0 and the time-periodic perturbation X_ε for $|\varepsilon|$ small. Recall that $\mathcal{P}_\varepsilon$ is the two-dimensional Poincaré map of X_ε, implying that $\mathcal{P}_0$ is the two-dimensional flow of X_0, which is very degenerate in the context of two-dimensional diffeomorphisms. We recall that periodic points of $\mathcal{P}_\varepsilon$ correspond to periodic solutions of X_ε, while $\mathcal{P}_\varepsilon$-invariant circles give rise to X_ε-invariant 2-tori.

We consider a number of dynamical properties of $\mathcal{P}_\varepsilon$, as these follow from more or less classical perturbation theory [3, 19, 20, 24, 37, 49]. First of all the hyperbolic periodic points (including fixed points) of $\mathcal{P}_0$ persist for $\mathcal{P}_\varepsilon$, for $\varepsilon \ll 1$, including their local stable and unstable manifolds. We note that globally the stable and unstable manifolds generically will behave different by separatrix splitting, giving rise to homo- and heteroclinic tangle. Secondly, the local bifurcations are persistent, in particular this holds for the saddle-node and cusp of periodic points but also for the Hopf bifurcations of these. In the latter case (for which the three-dimensional vector field X_ε gives Neĭmark-Sacker bifurcations), we encounter resonances due to the interaction of internal periodicity and that of the forcing. The strong resonances are more involved [3, 19, 20, 40, 52, 59], but in the case of weaker resonances, near the Hopf curve, the limit cycle turns into a $\mathcal{P}_\varepsilon$-invariant circle. In a corresponding two-dimensional section in $\mathcal{W}$, the associated rotation number is rational in a dense-open array of Arnol'd tongues emanating from the Hopf curve. Here the circle dynamics is of Kupka-Smale type [48], which corresponds to frequency locking with the periodic forcing. For a large measure set outside the tongues the invariant circles are quasi-periodic with Diophantine rotation number. The invariant circles break up further away from the Hopf curve in a complicated way, compare with [19]. The saddle-node bifurcation of limit cycles in X_0 turns into a quasi-periodic saddle-node bifurcation for $\mathcal{P}_\varepsilon$ [11, 12] with all the ensuing dynamical complexity [21–23], also compare with [14]. In a systematic study of the attractors of $\mathcal{P}_\varepsilon$ as a function of the parameters, we expect the same complexity as described in [13, 19, 20], for

more background also compare with [25,46,49,63]. In this investigation the present study of the autonomous system provides a skeleton. We come back to this in §1.4.2, regarding Rinaldi's model, compare with [52]. In this paper we restrict to the numerical detection of a few attractors of $\mathcal{P}_\varepsilon$ near homoclinic connections in the autonomous system X_0.

More precisely we consider the two-dimensional bifurcation diagrams of X_0, looking for the loci of homoclinic orbits (L_1 in Figure 4-(a) and L_1^a, L_1^b in Figure 4-(a)). These loci can be continued in the ε-direction for $\varepsilon \geq 0$. In particular we look in a neighbourhood of L_1 where complicated dynamics related to homoclinic tangencies are to be expected, compare with Figures 8, 9 and 10.

3. **Morse-Smale classification.**

This section discusses a topological classification of all possible Morse-Smale phase portraits for system (3). However, we first introduce a few necessary topological tools.

3.1. **Basic concepts.**

Our approach makes an extensive use of the Poincaré -Bendixson Theorem [48], which expresses that for planar vector fields all recurrence is trivial. We now describe a consequence of this theorem. Consider a smooth vector field X on a rectangle $T = PQRS$, such that the opposite sides PQ and RS are transversal to X and the other opposite sides PS and QR are tangent to X. Then, if X has no singularities inside T, the restriction $X|_T$ is smoothly conjugate to a standard flow-box.

A Morse-Smale vector field X is characterized as follows. All singularities (sinks, saddles and sources) and limit cycles of X are hyperbolic. Moreover X has no saddle-connections. We recall the fact [48] that a C^2-vector field X is Morse-Smale if and only if it is structurally stable. When restricting to a compact trapping domain, see §2.3, the set of Morse-Smale vector fields is open and dense in the C^2-topology.

We shall also heavily use index theory [44], which we briefly recall now. First the hyperbolic singularities have indices $\mathrm{ind}_p(X)$ as follows:

$$\mathrm{ind}_p(X) = \begin{cases} 1 \text{ if } p \text{ is a sink or source,} \\ -1 \text{ if } p \text{ is a saddle-point.} \end{cases}$$

Consider a bounded region D with a compact boundary ∂D. A smooth vector field X is defined on a neighbourhood of D with isolated singularities. We can define the index

$$i_D(X) = \sum_{X(p)=0,\, p\in \mathrm{int} D} \mathrm{ind}_p(X).$$

The Poincaré-Hopf Theorem [44] first asserts that for two vector fields X and $\tilde{X}$ as above, that coincide on an arbitrarily small neighbourhood of ∂D we have $i_D(X) = i_D(\tilde{X})$. Secondly the theorem states that for any smooth vector field X as above, that for each component of ∂D is either tangent or transversal, one has

$$i_D(X) = \chi(D),$$

where $\chi(D)$ is the Euler characteristic of D. We present two applications, to be used in the sequel.

As a first application again consider the rectangle $T = PQRS$, with a smooth vector field X which has the same behaviour on the boundaries as above. If X has no singularities in T, then clearly $i_T(X) = 0$. This implies that $i_T(X) = 0$ also for

cases where X does have singularities in T. A second application concerns the case where D is a disc with a smooth vector field X, which is either tangent or transverse to the boundary ∂D. In both cases $i_D(X) = \chi(D) = 1$.

3.2. **Number of singularities.** Our study concerns the closed first quadrant $\mathrm{clos}(\mathcal{Q}) = \{x \geq 0, y \geq 0\}$ and $(\alpha, \beta, \mu, \delta, \lambda) \in \mathcal{W} \times \Delta$, where $\mathcal{W} = \{\beta > -2\sqrt{\alpha}, \alpha \geq 0, \mu \geq 0\}$ and $\Delta = \{\delta > 0, \lambda > 0\}$. Denote by $X = X_{\delta,\lambda,\alpha,\beta,\mu}(x, y)$ the family of vector fields (3). First, X possesses several singularities (equilibria) on the axes.

1. Since $\delta > 0$, the origin $\mathrm{O} = (0, 0)$ is a hyperbolic saddle-point with $\{x = 0, y > 0\} \subset W^s(0)$ and $\{y = 0,\ x < 1/\lambda\} \subset W^u(0)$.
2. Since $\mu \geq 0$, the singularity $E = (0, -\delta/\mu)$ is below the x-axis.
3. The singularity $\mathrm{C}_\lambda = (\frac{1}{\lambda}, 0)$ will play a central role. The eigenvalues of $DX(\mathrm{C}_\lambda)$ are $(-\delta, \Lambda)$, where

$$\Lambda = \frac{\lambda}{\alpha + \lambda(\beta + \lambda)} - \delta.$$

This implies that generically C_λ is either a sink ($\Lambda < 0$) or a saddle-point ($\Lambda > 0$). Observe that $\{y = 0, x \geq 0\} \subset \mathrm{clos}(W^s(\mathrm{C}_\lambda))$. Although C_λ is persistent, it is really semi-hyperbolic when

$$\alpha - \frac{\lambda}{\delta} + \lambda(\beta + \lambda) = 0.$$

Colloquially speaking, C_λ is the only point from which singularities enter or leave $\mathcal{Q}$. The corresponding bifurcation is a *transcritical bifurcation*, see §4.1 for details.

Our search for singularities now concerns $\mathcal{Q}$. From (3) a singularity (x, y) must satisfy

$$\begin{cases} y &= (1 - \lambda x)(1 + \beta x + \alpha x^2), \\ 0 &= -\delta(1 + \beta x + \alpha x^2) - \mu(1 - \lambda x)(1 + \beta x + \alpha x^2)^2 + x. \end{cases} \tag{7}$$

Therefore, the singularities of X correspond to the zeroes of

$$F_{\alpha,\beta,\mu,\delta,\lambda}(x) = -\delta(1 + \beta x + \alpha x^2) - \mu(1 - \lambda x)(1 + \beta x + \alpha x^2)^2 + x. \tag{8}$$

In §4 we shall see that $F(x) = F_{\alpha,\beta,\mu,\delta,\lambda}(x)$ does not have more than three singularities.

3.3. **Compact trapping domain.** We may restrict the domain of the phase portrait to an invariant subset of $\mathcal{Q}$ where all trajectories of X enter and do not leave again, called a trapping domain. In what follows, X_t denotes the flow of X over time t.

Proposition 1. (Trapping domain) *For all $(\alpha, \beta, \mu, \delta, \lambda) \in \mathcal{W} \times \Delta$, and for all p such that*

$$p > \frac{1}{\lambda}\left(\frac{1}{4\delta}(1 - \delta)^2 + 1\right),$$

the compact domain defined by

$$\mathcal{B}_p = \{(x, y) \mid x + y \leq p,\ x \geq 0,\ y \geq 0\}$$

is invariant under X_t for all $t \geq 0$ and therefore is a trapping domain.

Observe that $\mathcal{B}_p$ contains C_λ and does not depend on (α, β, μ).

Proof. We show that for p sufficiently large, the function

$$(x, y) \mapsto F_p(x, y) = x + y - p$$

is a Lyapunov function. For each p, consider the line

$$L_p = \{(x, y) \mid x \geq 0,\ y \geq 0,\ F_p(x, y) = 0\}.$$

Since the axes are invariant under X_t, it is sufficient to show that $X(F_p) < 0$. From (3) we get

$$X(F_p) = x - \lambda x^2 - \delta y - \mu y^2.$$

We shall show that there exists $p > 0$ such that the map

$$f : L_p \to \mathbb{R},\ (x, y) \mapsto x - \lambda x^2 - \delta y$$

is negative. The boundary of L_p consists of two points $(0, p)$ and $(p, 0)$ where $f(0, p) = -\delta p < 0$ and by taking $p > 1/\lambda$, we have $f(p, 0) = p - \lambda p^2 < 0$. So, f is negative at the boundary of L_p. This implies the following: if f changes sign on L_p, f possesses a global maximum, i.e., there exists $(x_2, y_2) \in L_p$ such that

$$f(x_2, y_2) = \sup_{(x,y)\in L_p} f(x, y),\ x_2 > 0,\ y_2 > 0.$$

At (x_2, y_2) the following equality holds

$$df(x_2, y_2) \wedge dF_p(x_2, y_2) = 0,\ \text{i.e.,} \begin{vmatrix} 1 - 2\lambda x_2 & -\delta \\ 1 & 1 \end{vmatrix} = 0.$$

This further implies that

$$y_2 = p - \frac{1 + \delta}{2\lambda},\ x_2 = \frac{1 + \delta}{2\lambda},$$

and

$$\begin{aligned} f(x_2, y_2) &= \frac{1 + \delta}{2\lambda} - \lambda\left(\frac{1 + \delta}{2\lambda}\right)^2 - \delta\left(p - \frac{1 + \delta}{2\lambda}\right) \\ &= \frac{1}{4\lambda}(1 - \delta)^2 + \frac{\delta}{\lambda}(1 - p\lambda), \end{aligned} \tag{9}$$

which is negative if

$$p > \frac{1}{\lambda}\left(\frac{1}{4\delta}(1 - \delta)^2 + 1\right).$$

□

3.4. **Surgery.** Given a smooth vector field X defined on a bounded annulus A, without singularities, which is transversal to the boundary ∂A. Assume that the annulus allows a global transversal (radial) section Σ, on which the Poincaré return map is well-defined. As a consequence of the Poincaré-Bendixson and the Poincaré-Hopf Theorems (see §3.1), we conclude that the only invariant sets inside A are limit cycles that are 'parallel' to the boundary. A next observation deals with the orientation of X at the boundary ∂A. If at one boundary component X points inward and at the other outward, the number of limit cycles is even. In all other cases, this number is odd.

We shall describe the result of a surgery [47] on such an annulus, where we assume that the set of limit cycles of X inside, is maximal with respect to inclusion. Consider the complement $\mathbb{R}^2 \backslash A$, which has two components, an inner part $\mathcal{I}$ which is a disc and an outer part $\mathcal{O}$. Assuming that X is Morse-Smale, we claim the following.

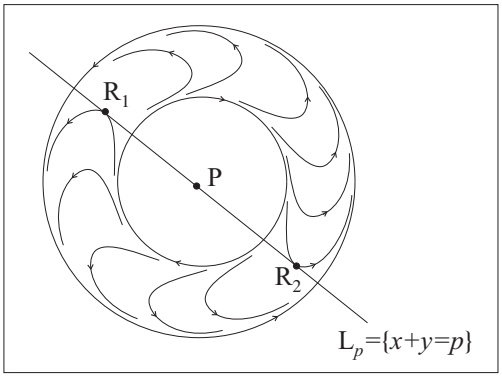

FIGURE 12. A 'Reeb component' [35] does not occur in our system.

There exists a new smooth vector field Y, which is again Morse-Smale, such that $Y|_{\mathcal{O}} = X|_{\mathcal{O}}$ and $Y|_{\mathcal{I}} = \pm X|_{\mathcal{I}}$, where we take the plus-sign if the number of limit cycles is even and the minus-sign otherwise. Moreover Y has neither singularities nor limit cycles inside A. In fact, the restriction $Y|_A$ is conjugate to the 'radial' vector field of A. In order to apply the above to our situation we need the following.

Proposition 2. *Given limit cycles* Γ *and* Γ' *that bound an annulus without singularities and other limit cycles, then* Γ *and* Γ' *have the same orientation.*

Proof. Assume that system (3) possesses two limit cycles Γ, Γ' that bound an annulus without singularities and other limit cycles, but with different orientation. By an index argument we find a singular point $\mathrm{P} = (\mathrm{P}_x, \mathrm{P}_y)$ of X in the inner part $\mathcal{I}$ of the annulus. Take $p \in \mathbb{R}$ such that the line $\mathrm{L}_p = \{x + y = p\}$ passes through $\mathrm{P} = (\mathrm{P}_x, \mathrm{P}_y)$. As the orientation of Γ and Γ' are different, L_p contains two points $\mathrm{R}_1 = (\mathrm{R}_{1,x}, \mathrm{R}_{1,y})$ and $\mathrm{R}_2 = (\mathrm{R}_{2,x}, \mathrm{R}_{2,y})$ distinct from P where the flow associated to X is tangent to L_p, see Figure 12. Taking the directional derivative $X(x + y) = d(x + y)(X)$ we find

$$d(x + y)(X) = x - \lambda x^2 - \delta y - \mu y^2 = 0,$$

which means that the three points P, R_1 and R_2 must satisfy

$$\begin{aligned} 0 &= x - \lambda x^2 - \delta(p - x) - \mu(p - x)^2 \\ y &= p - x. \end{aligned} \tag{10}$$

Note that (10) is an equation of degree 2 and therefore has no more than two solutions which contradicts the fact that (10) must be valid for three different values of x. □

As a consequence of this proposition and the Poincaré-Bendixson Theorem (see §2.1) we claim that any limit cycle Γ of X is contained in an annulus A which is maximal in the above sense.

Note that after a surgery we get a smooth vector field. If we have another annulus, we apply the surgery to the new vector field and obtain again another smooth vector field. We keep doing these surgeries until we have a smooth vector field without limit cycle. As mentioned at the beginning of this section, the vector field to be considered is of Morse-Smale type. This implies that we only have a finite number of limit cycles. Therefore, after finitely many surgeries we change X

into a vector field without limit cycles Y = Red(X), called Reduced Morse-Smale vector field.

3.5. **Topological classification.** We start the topological classification of the reduced Morse-Smale vector field Y. Throughout we assume that Y has the trapping domain $\mathcal{B}_p$, including the fact that $(0,0)$ is a hyperbolic saddle-point and that $\mathrm{C} = (c,0)$ is a singularity, with $0 < c < p$. The axes are invariant, where $W^s(0,0) = \{x = 0\}$, $W^u(0,0) = \{y = 0, x < c\}$ and $\{x > 0\} \subseteq W^s(\mathrm{C})$. Also we assume that Y in $\operatorname{int}\mathcal{B}_p$ has no more than three singularities. Compare with Corollary 1 in §4.

Lemma 1. (Type of singularities) *In the above circumstances, the reduced Morse-Smale vector field Y has the following possible configurations of singular points, apart from $(0,0)$ and* C.

1. *If* C *is a sink, then there are either zero or two singularities. In the latter case, the singularities are either a saddle-point* S *and a sink* A, *or a saddle-point* S *and a source* R.
2. *If* C *is a saddle-point, then there are either one or three singularities. Always one of the singularities is a sink* A_0 *and in the latter case we have either a saddle-point* S *and a sink* A, *or a saddle-point* S *and a source* R.

Proof. First assume that C is a sink. We construct a 'rectangle' $T = PQRS$ inside $\mathcal{B}_p$ as follows. The side RS is on the hypothenuse of $\mathcal{B}_p$ and therefore transversal to Y. The side PQ is situated near C, also transversal to Y. The sides PS and QR are segments of integral curve of Y, see Figure 13. Note that we can choose T such that all singularities (except $\mathrm{O} = (0,0)$ and $\mathrm{C} = (c,0)$) of Y are inside T. This follows from the fact that the sides PS and QR can be chosen arbitrarily close to the coordinate axes. As shown in §3.1, the index $i_T(Y) = 0$. From this the proof of the present part is immediate.

Now assume that C is a saddle-point. First apply the Poincaré-Bendixson Theorem (§3.1), implying that $W^u(\mathrm{C})$ converges to a sink A_0. Taking a neighbourhood of $W^u(\mathrm{C})$ that is transversal to Y, we replace the lower arc PQ of the rectangle T by the boundary of this neighbourhood, see Figure 13. This gives a similar rectangle T' to which the above argument applies again. □

Proposition 3. (Classification without limit cycles) *In the above circumstances, there are six topological classification of phase portraits of the reduced Morse-Smale vector field Y, listed in Figures 2-(a) and 2-(b).*

Remark. The phase portraits of Figure 2-(a) belong to the case where C is a sink and those of Figure 2-(b) to the case where C is a saddle-point. Note that the latter case is obtained from the former, by pushing the sink C inside $\operatorname{int}\mathcal{B}_p$ in the position A_0. Compare with the proof of Lemma 1. Note that bi-stability only occurs in the cases [a-2] and [b-2].

Proof. Case where C is a sink: First assume that apart from $(0,0)$ and C there are no singularities. Using the rectangle T of Lemma 1 and the consequence of the Poincaré-Bendixson Theorem mentioned in §3.1 we end up with a flow-box and hence obtain case [a-1].

Second, from Lemma 1 we know the possibilities of the singularities. In the case with a saddle-point S and a sink A, consider the stable manifolds $W^s(\mathrm{S})$ that act as

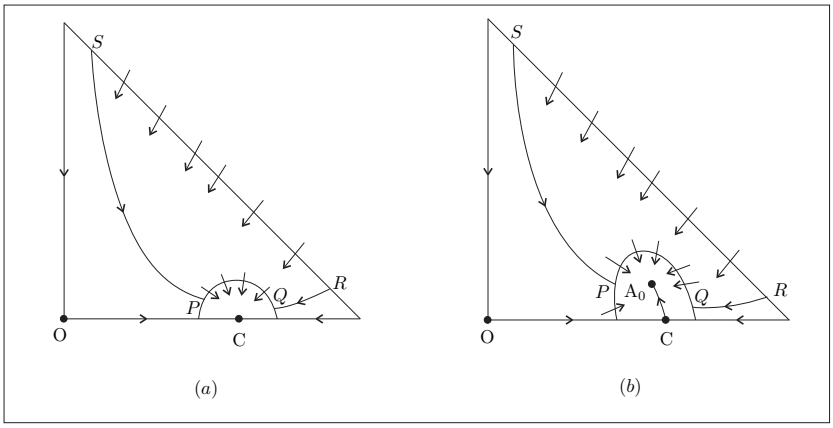

FIGURE 13. Rectangle $T = PQRS$ inside $\mathcal{B}_p$ of index 0, containing all singularities (except $(0,0)$ and C): (a): Case where C is a sink. (b): Case where C is a saddle-point.

separatrices. Using the Poincaré-Bendixson Theorem, there is no α-limit set inside $\mathcal{B}_p$ and hence both arcs have to come from the hypothenuse of $\mathcal{B}_p$. This leaves us with the case [a-2]. Note that the two arcs of $W^s(\mathrm{S})$ separate the basins of the attractors A and C. Next we consider the case of Lemma 1 with a saddle-point S and a source R. Considering the unstable manifolds $W^u(\mathrm{S})$, there is only one possible ω-limit set, namely the point C. This is the case [a-3].

CASE WHERE C IS A SADDLE-POINT: We repeat the procedure in the proof of Lemma 1, taking a neighbourhood $W^u(\mathrm{C})$. In the complement of this neighbourhood, the first part of the present proof applies. The case [b-j] so corresponds to [a-j] for $j = 1, 2$ and 3. □

How to return from the Reduced Morse-Smale vector field Y to the original Morse-Smale vector field X? Recall that Y was obtained from X by surgery, where each maximal annulus was replaced by an annulus with a radial vector field. Therefore, after reduction from X to Y, each maximal annulus of X corresponds to an isotopy class of Y-transversal curves. Such a transversal curve bounds a disc D with index $i_D(Y) = 1$. By examining all of the six cases of Figures 2-(a) and 2-(b) we get the following.

Proposition 4. (GENERAL CLASSIFICATION) *Given the type of Y, the maximal annuli for X can be re-inserted as follows:*

Case a:

1. *No annulus possible;*
2. *The annulus is to be put around the point* A;
3. *The annulus is to be put around the point* R.

Case b:

1. *The annulus is to be put around the point* A_0;
2. *The annuli are to be put around the point* A_0 *or around the point* A, *or around all singularities* A_0, S *and* A;
3. *The annuli are to be put around the point* A_0 *or around the point* R, *or around all singularities* A_0, S *and* R.

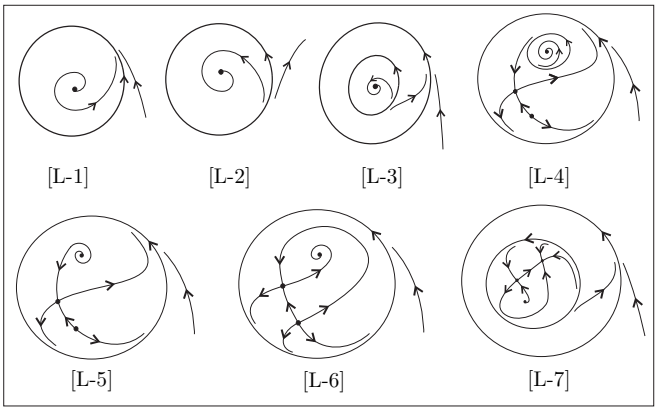

FIGURE 14. Dynamics associated to limit cycles as detected numerically in (3). In particular, numerically we find at most two limit cycles.

Each annulus may contain an arbitrary non-negative number of limit cycles (including the number 0) and the topological type of X only depends on the topological type of Y and these numbers.

Remark. We recall that we may have to change the sign of Y in the inner regions $\mathcal{I}$ of the annuli, according to the parity of the number of limit cycles. Note that this may have to be done repeatedly.

All possible configurations associated to limit cycles, that we detected numerically are summarized in Figure 14.

4. **Bifurcations and organizing centres.** We now describe all bifurcations occurring in system (3) concerning the trapping domain $\mathcal{B}_p$, see Table 1 for an exhaustive list of the bifurcations [28, 29, 37, 41]. This list involves bifurcations of singularities, homoclinic orbits and limit cycles. All local singularities unfold generically in the parameter space, which can be checked algebraically. Our proof of Theorem 2 is based on these investigations. We refer to [17, 56] for details.

4.1. **Transcritical bifurcation and its degeneracy.** We discuss a scenario in which a singularity enters or leaves the trapping domain via the singularity C $= (1/\lambda, 0)$. Recall that the family (3) depends on five parameters $\alpha, \beta, \mu, \delta$ and λ, where

$$(\delta, \lambda) \in \Delta = \{\delta > 0, \lambda > 0\} \text{ and } (\alpha, \beta, \mu) \in \mathcal{W} = \{\beta > -2\sqrt{\alpha}, \alpha \geq 0, \mu \geq 0\}.$$

As mentioned in §3.2, the singularity C is a hyperbolic singularity at the boundary $\partial\mathcal{Q}$, which becomes transcritical when the eigenvalue transversal to the x-axis becomes zero, see [37, 41]. Since $\dim \mathcal{W} = 3$ we have to study degenerate and doubly degenerate versions as well. The bifurcation set in $\mathcal{W}$ near TC_3 is depicted in Figure 16. We state the following proposition.

Proposition 5. (TRANSCRITICAL BIFURCATION) *For all $(\delta, \lambda) \in \Delta$, the associated bifurcation set of* (3) *in $\mathcal{W}$ possesses a codimension* 3 *transcritical point* TC_3*, a codimension* 2 *transcritical curve* TC_2 *and a codimension* 1 *transcritical surface*

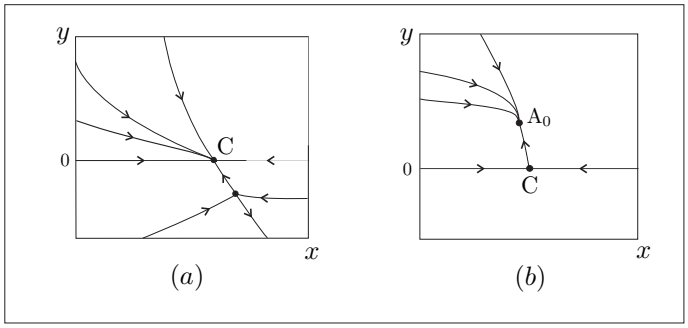

FIGURE 15. A scenario of the codimension 1 transcritical bifurcation (TC_1). (a): Before TC_1. (b): After TC_1, a new equilibrium A_0 enters $\mathcal{Q}$ via C.

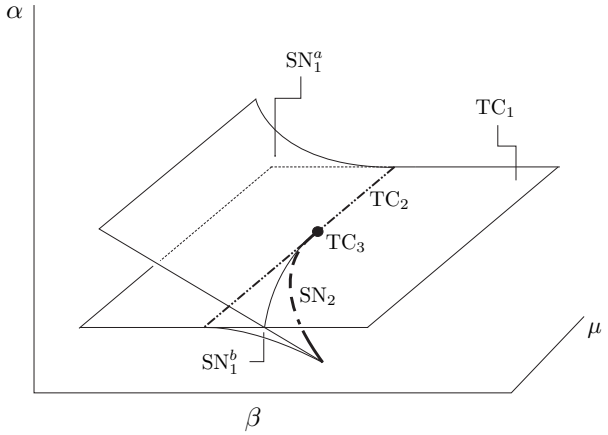

FIGURE 16. Local geometry of codimension 3 transcritical point (TC_3).

TC_1, *where all bifurcations are generic. Their union is a smooth plane* TC. *No further degeneracy occurs.*

The proof of this proposition is a straight-forward application of the classical normal form theory [8,37,60], using some computer algebra (Mathematica [66]), for details see [17, 56].

Now we study the bifurcations occurring in the interior of $\mathcal{B}_p$.

4.2. **Saddle-node and cusp bifurcations.** We have the following.

Proposition 6. (SADDLE-NODE BIFURCATION) *For all* $(\delta, \lambda) \in \Delta$*, the corresponding bifurcation set of* (3) *in* $\mathcal{W}$ *possesses two saddle-node surfaces which are subordinate to a smooth cusp curve* SN_2.

As in the case of Proposition 5, the proof is a straight-forward application of the classical normal form theory [8,37,60], using some computer algebra (Mathematica [66]), see [17,56] for details.

Note that since SN_2 is connected, it is subordinate to TC_3. We now investigate Hopf bifurcation and its degeneracy.

4.3. **Hopf bifurcation and its degeneracy.** We state the following proposition.

Proposition 7. (HOPF BIFURCATION) *For all* $(\delta,\lambda)\in\Delta$*, the corresponding bifurcation set of* (3) *in* $\mathcal{W}$ *possesses a smooth connected surface of Hopf bifurcations* (H)*. Furthermore when* $(\delta,\lambda)\in\Delta_1$*, there are two smooth connected curves of codimension* 2 *Hopf bifurcations* (H_2^a *and* H_2^b) *on the surface* H*. The complement* $\mathrm{H}_1=\mathrm{H}\setminus(\mathrm{H}_2^a\cup\mathrm{H}_2^b)$ *corresponds to Hopf bifurcation of codimension* 1*. However, when* $(\delta,\lambda)\in\Delta_2$*, there is only one smooth connected curve of codimension* 2 *Hopf bifurcations* H_2 *on the surface* H*. Again* $\mathrm{H}_1=\mathrm{H}\setminus\mathrm{H}_2$.

We note that both curves H_2^a and H_2^b are subordinate to codimension 3 points BT_3, NF_3^a and NF_3^b to be investigated in §4.4, see Figure 3. Again the proof of this proposition is a straight-forward application of classical normal form theory [8, 37, 60], using some computer algebra (Mathematica [66]), see [17, 56] for details.

4.4. **Bogdanov-Takens bifurcation and its degeneracy.** The following propositions describe how the set of Bogdanov-Takens bifurcations is organized and locally stratified.

Consider system (3) near a singularity (x_0,y_0) at which the eigenvalues of the linear part are purely imaginary. For convenience, we introduce complex coordinates $z=(x-x_0)+i(y-y_0)$ in a neighbourhood of (x_0,y_0) and compute the normal form. We have

$$\dot z = (H_1+iw)z+\mathcal{O}(|z|^3), \tag{11}$$

where H_1 and w depend algebraically on the parameters. Consider the map

$$\begin{aligned}\mathcal{F}:\mathcal{W}\times\Delta\times\mathbb{R}_+ &\to \mathbb{R}^5\\ (\alpha,\beta,\mu,\delta,\lambda,x) &\mapsto \Big(F(x),F'(x),H_1(\alpha,\beta,\mu,\delta,\lambda),\delta,\lambda\Big)\end{aligned} \tag{12}$$

where F is defined in (8) and H_1 in (11). For all $(\delta,\lambda)\in\Delta$, we write

$$\mathrm{N}=\{\pi\mathcal{F}^{-1}(0,0,0,\delta,\lambda)\},$$

which is a smooth curve containing all nilpotent singularities of system (3).

Proposition 8. (BOGDANOV-TAKENS BIFURCATION) *For all* $(\delta,\lambda)\in\Delta$*, the bifurcation set of* (3) *in* $\mathcal{W}$ *possesses a smooth curve* N *of nilpotent singularities of system* (3)*. An open and dense subset of* N *is formed by a Bogdanov-Takens curve* BT_2 *which is subordinate to a single codimension* 3 *Bogdanov-Takens point* BT_3.

We refer to [28] for a description of the geometry and stratification near a Bogdanov-Takens point BT_3.

Proof. We investigate higher degeneracies of the Bogdanov-Takens bifurcation BT_2. We look at the germ associated to (3) near the corresponding singularity (x_0,y_0). Setting $u=x-x_0, v=y-y_0$, on the set N, the corresponding germ has a 4-jet C^∞ conjugate to [28, 29, 61]

$$\begin{aligned}\dot u &= v,\\ \dot v &= K_1u^2+K_2uv+K_3u^3+K_4u^2v+K_5u^4+K_6u^3v,\end{aligned} \tag{13}$$

where for each $i=1,\dots,6$, the coefficient K_i depends on the parameters, see [56] for details. The Bogdanov-Takens bifurcation BT_2 is nondegenerate when $K_1\neq 0$ and $K_2\neq 0$. Further degeneracy occurs when $K_1=0$ or $K_2=0$ [28, 29]. Now we

investigate the case when $K_2 = 0$ and $K_1 \neq 0$ which corresponds to BT_3. Consider the map

$$\begin{aligned} \mathcal{F}_d : \mathcal{W} \times \Delta \times \mathbb{R}^+ &\rightarrow \mathbb{R}^6 \\ (\alpha, \beta, \mu, \delta, \lambda, x) &\mapsto \Big(F(x), F'(x), H_1, K_2, \delta, \lambda \Big). \end{aligned}$$

This map can be algebraically checked to be a local diffeomorphism near

$$\mathcal{F}_d^{-1}\{(0,0,0,0,\delta,\lambda),\ |\ (\delta,\lambda) \in \Delta\}.$$

Moreover, another algebraic nondegeneracy condition has to be verified [29]. These two conditions imply that for all $(\delta, \lambda) \in \Delta$, the bifurcation set in $\mathcal{W}$ contains an isolated BT_3 point in N to which BT_2 is subordinate. □

In the following proposition we discuss the case when $K_1 = 0$ and $K_2 \neq 0$ which leads to a singularity of nilpotent-focus type NF_3 [29]. The proof of the proposition is partially based on numerical results. Mathematically, the local bifurcations are well understood. However, to get a full picture of the bifurcations with the connection between organizing centres is in general a very hard task. Therefore computer assistance is needed. More details are given in [17].

Proposition 9. (Singularity of nilpotent-focus type)

1. *There exists a smooth, algebraic curve* $\mathcal{C} \subset \Delta$, *which separates* Δ *into two parts* Δ_1 *and* Δ_2. *For all* $(\delta, \lambda) \in \Delta_1$ *the curve* N *contains two nilpotent-focus singularities* NF_3^a *and* NF_3^b, *while for all* $(\delta, \lambda) \in \Delta_2$ *the curve* N *contains no such points.*
2. *Recall the projection* $\Pi : \mathcal{W} \times \Delta \rightarrow \Delta$. *The closure of the set* $\mathcal{N} \subset \mathcal{W} \times \Delta$ *consisting of parameter values for which system* (3) *has a singularity of nilpotent-focus type* (NF_3) *is a smooth surface with a generic projection under* Π.

We refer to [29] for a description of the geometry and stratification near NF_3. We remark that all singularities on the curve N are listed in the Propositions 8 and 9.

Proof. Applying a linear scaling on u and v of the form

$$u = A\bar{u}, \quad v = A\bar{v}, \quad A = \pm\frac{1}{\sqrt{K_3}},$$

the 4-jet (13) reads

$$\begin{aligned} \dot{u} &= v, \\ \dot{v} &= AK_1u^2 + AK_2uv \pm u^3 + A^2K_4u^2v + A^3K_5u^4 + A^3K_6u^3v. \end{aligned} \tag{14}$$

Consider the map

$$\begin{aligned} \mathcal{F}_n : \mathcal{W} \times \Delta \times \mathbb{R}^+ &\rightarrow \mathbb{R}^6 \\ (\alpha, \beta, \mu, \delta, \lambda, x) &\mapsto \Big(F(x), F'(x), H_1, K_1, \delta, \lambda \Big). \end{aligned}$$

Let

$$\mathcal{J} = \det(\mathrm{D}\mathcal{F}_n)(\alpha, \beta, \mu, \delta, \lambda, x),$$

and define the map

$$\begin{aligned} \mathcal{C}_n : \mathcal{W} \times \Delta \times \mathbb{R}^+ &\to \mathbb{R}^5 \\ (\alpha, \beta, \mu, \delta, \lambda, x) &\mapsto \Big(F(x), F'(x), H_1, K_1, \mathcal{J} \Big). \end{aligned}$$

By a computer assisted investigation it follows that the map $\mathcal{C}_n$ is a submersion near $\mathcal{C}_n^{-1}\{0\}$, which is a connected and smooth curve in $\mathcal{W} \times \Delta$. The curve $\mathcal{C}$ now is obtained as the projection of $\mathcal{C}_n^{-1}\{0\}$ under $(\alpha, \beta, \mu, \delta, \lambda, x) \mapsto (\delta, \lambda)$. This projection is a smooth curve that splits Δ into two open regions Δ_1 (below $\mathcal{C}$) and Δ_2 (above $\mathcal{C}$), see Figure 13. For all $(\delta, \lambda) \in \Delta_1$, our investigation reveals that the set $\pi \circ \mathcal{F}_n^{-1}\{(0, 0, 0, 0, \delta, \lambda)\}$ consists of two singularities of nilpotent-focus type [28] NF_3^a and NF_3^b that collide as (δ, λ) approaches the curve $\mathcal{C}$ and disappear when $(\delta, \lambda) \in \Delta_2$ in a generic fold. □

Corollary 1. *System* (3) *has no more than three singularities in* $\mathcal{Q}$.

Proof. The proof follows from the bifurcation analysis done in §4.1 and §4.2. More precisely for all $(\delta, \lambda) \in \Delta$ and for all $\mu \geq 0$, from Propositions 5 and 6 we have the following diagram in the (α, β)-plane, see Figure 17. This figure contains *the* part of the bifurcation diagram that organizes the number of singularities, independent of (δ, λ). There are only two possible scenarios as shown in diagrams (a) and (b) of Figure 17 depending on the value of μ. In the upper right region of both diagrams the number of singularities is zero and we can attain any other parameter point with a Morse-Smale system, by a path that crosses no more than three curves of codimension 1.

We emphasize that all computations needed to obtain this information are of algebraic nature, although the checks are computer assisted. □

4.5. **Global bifurcations.** We discuss here the global aspects of the dynamics occurring in system (3), i.e., limit cycles and homoclinic connections. Also we describe different bifurcation features that involve both local and global aspects of the dynamics. Our approach is mainly numerical.

Limit cycles. As known in bifurcation theory [37,41], limit cycles may come into existence by Hopf bifurcation H_1, saddle-node bifurcation of limit cycles SNLC_1, homoclinic bifurcations L_1 and by their various degeneracies. With help of Matlab [38] and Matcont [36], we detect and continue limit cycles in system (3), see for instance regions 3, 6, 8 and 9 in Figure 5-(c).

Homoclinic and saddle-node homoclinic bifurcations. A homoclinic connection mostly occurs as the continuation of a Bogdanov-Takens bifurcation, which is detected with the help of AUTO2000 [27]. Using this tool, we also can detect a branch of saddle-node homoclinic bifurcation , i.e., a saddle-node bifurcation on a limit cycle [37, 41]. This scenario for instance occurs in the transition between regions 9 and 3 in Figures 4-(b) and 4-(c).

5. Concluding remarks.

5.1. **Biological aspects.** We now discuss a few biological interpretations of our results regarding model (3). Globally speaking there are three possibilities for the coexistence of predators and prey. In the first case the parameters are below the transcritical curve TC_1, compare with Figures 5, 12 and 15, which implies that C is a saddle-point. Therefore, independent of the initial values in $\mathcal{Q}$, both prey and

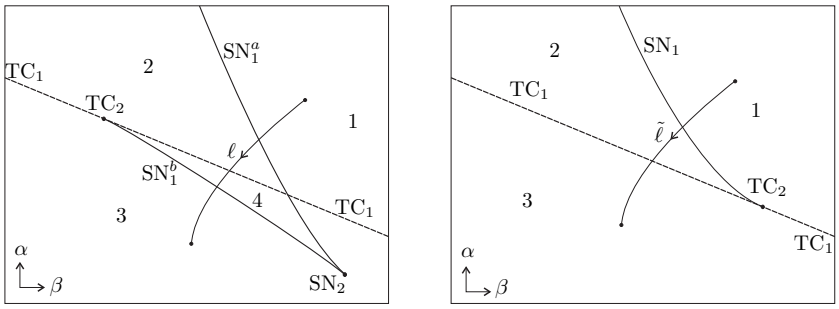

(*a*) (*b*)

FIGURE 17. (*a*): Bifurcation set in two-dimensional section Σ_1 of Figure 16 transversal to the curve TC_2 close to TC_3, compare Figures 4-(*b*) and 4-(*c*). For parameter values in region 1, there are no singularities. We now follow a path ℓ from region 1, via regions 2 and 4 to region 3. Since ℓ crosses the curve SN_1^a, two singularities occur in region 2. Another singularity enters $\mathcal{Q}$ via TC_1, thus there are three singularities in region 4. Two of these singularities disappear in region 3 via SN_1^b. (*b*): Bifurcation set in two-dimensional section Σ_2 of Figure 16 transversal to the curve TC_2 close to TC_3 but on the opposite side of Σ_1, compare Figure 5-(*c*). For parameter values in region 1, there are no singularities. Similar to the discussion on diagram (*a*), we conclude that, since $\tilde{\ell}$ crosses the curve SN_1, two singularities occur in region 2. One of these two singularities leaves $\mathcal{Q}$ via TC_1. For terminology see Table 1.

predators survive. Compare with regions 3 and 5 in Figure 4-(*a*). In the second case, only the prey survives, compare with region 4 in Figure 4-(*a*). In the last case, depending of the initial values in $\mathcal{Q}$, only the prey survives or both prey and predators survive (bi-stability). As an example see region 12 in Figure 4-(*a*).

On the role of the parameters. From the biological point of view, the coefficients δ, λ and μ play the role of parameters. Some anthropic activities (agriculture, fishery) can modify the values of these parameters. For example, $1/\lambda$ is proportional to the carrying capacity of the prey, which is the amount of prey that the environment may sustain. This depends on the nutrient richness (nitrate, phosphate, etc). If the prey consists of nutrient consumers, any enrichment of the environment by an increase of the nutrient supply may increase the carrying capacity and thus decrease the value of λ. When dealing with the management of the environment, one often tries to reduce the amount of nitrate or phosphate in the environment, giving an increase of the parameter λ. The other parameters (α and β) are linked to behavioural or physiological properties of the organisms, such as that of group defence or physiological saturation, and can not be easily changed.

We now present a few related models as these partly appear in the literature, indicating possible relationships with the present approach.

5.2. **Time-periodicity.** We start discussing aspects of the time-periodic model, i.e., the forcing (4) applied to (3). Biologically this means that the carrying capacity varies periodically, which is related to the competition amongst prey for special

niches or epidemics. As stated in §2.2, we find several strange attractors regarding this forced model, compare with Figures 8, 9 and 10. A more systematic approach of this and related time-periodic systems is subject of future research.

Rinaldi *et al.* [52] give six options for a time-periodic set-up. One of these consists of Bazykin's model with forcing (4) when next to $\alpha = 0$, one also sets $\mu = 0$. The corresponding bifurcation set for the autonomous system of this setting is obtained from Figure 5-(a) by considering the line $\{\mu = 0\}$ which contains two Hopf points Q^a and Q^b. Moreover, the periodic forcing is in $1:2$ resonance with the periodic motion of one of the Hopf limit cycles at the moment of bifurcation. A strange attractor is detected near a limit cycle. Compare with the attractors of our model in Figures 8, 9 and 10. Besides (4), one may set

$$a = a_0 \left(1 + \varepsilon \sin\left(\frac{2\pi}{\omega} t\right)\right)$$

which expresses seasonal fluctuation of the growth rate. Also putting

$$m = m_0 \left(1 + \varepsilon \sin\left(\frac{2\pi}{\omega} t\right)\right)$$

expresses that also the harvest rate of the predator fluctuates during the year, see [52] for details.

These various settings will be incorporated in the program announced above in the full generality of (3), including exponential response functions like (5) and following the general strategy of [19, 20].

Remark. One may apply quasi-periodic forcing to system (3). In this case, local bifurcations in (3) give rise to quasi-periodic bifurcations [11, 12]. In the case of Hopf bifurcation, resonances are encountered between frequencies of the internal and the forcing periodicity [57, 64].

5.3. **Infinite dimensional variations.** In Volterra-Lotka like models of population dynamics often aspects are taken into account which go beyond the framework of ordinary differential equations. We are thinking of time-delay or spatial effects and of noise. We briefly discuss this in the context of the present model (3).

1. In natural populations, there is a time-delay in reproduction. For instance the birth rate of prey depends on the population at the time $t - \tau$ where $\tau > 0$. In May [43], this leads to the following system
$$\begin{aligned} \dot{x}(t) &= ax(t-\tau) - \lambda x^2(t) - by(t)x(t) \\ \dot{y}(t) &= -\delta y(t) + x(t)y(t) \end{aligned}$$
where $b > 0$. In most cases this delay is significant and the model reacts different from the instantaneous case [51] where periodic solutions can change from stable to unstable. Complicated dynamics are observed in [43, 50].
2. Another aspect that system (3) does not take into account is the fact that populations have a space distribution $x = x(u,t), y = y(u,t)$, where $u = (u_1, u_2)$. For instance, if a large amount of prey or predators is crammed into a certain area, a tendency exists to diffusion. For instance if we consider the diffusion, system (3) leads to the following system
$$\begin{aligned} \frac{\partial x}{\partial t} &= D_1 \mathbf{\Delta}_u(x) + x(a - \lambda x) - yP(x) \\ \frac{\partial y}{\partial t} &= D_2 \mathbf{\Delta}_u(y) + y(-\delta - \mu y + cP(x)), \end{aligned}$$

where D_1 and D_2 are diffusion coefficients of prey and predator, respectively. In several reaction-diffusion systems modelling predator-prey interactions, chaotic dynamics are observed [26, 30, 43].

3. Also a stochastic term can be added to (3) with forcing (4), i.e., leading to

$$\begin{aligned} dx &= (x(a-\lambda(t)x) - yP(x))dt + b_1(x,y,t)dW_1(t) \\ dy &= y(-\delta - \mu y + cP(x))dt + b_2(x,y,t)dW_2(t), \end{aligned}$$

where $dW_1(t)$ and $dW_2(t)$ are Brownian motions. One may expect fluctuational transitions between two co-existing attractors as observed in several discrete dynamical systems [9, 45, 55].

It will be of interest to study the general system (3) including one (or more) of these three aspects with special interest in the stability of periodic solutions, the transition between attractors and the complexity of the dynamics.

Acknowledgements. The authors like to thank Odo Diekmann, Bernd Krauskopf, Kurt Lust, Jean-Christophe Poggiale and Floris Takens for helpful discussions.

REFERENCES

[1] R. Abraham and J.E. Marsden, "Foundations of Mechanics," Benjamin Cummings, 1978.
[2] J. F. Andrews, *A mathematical model for the continuous of microorganisms utilizing inhibitory substatrates*, Biotechnol. Boieng., **10** (1968), 707–723.
[3] V.I. Arnold, "Mathematical Methods of Classical Mechanics," Springer-Verlag GTM **60**, 1980.
[4] B. Barnes and H. Sidhu, *Plant-herbivore models, where more grass means fewer grazers*, Bull. of Math. Biol., **67** (2005), 33–55.
[5] A.D. Bazykin, *Nonlinear dynamics of interacting populations*, in "World Scientific Series on Nonlinear Sciences A 11" (ed. A.I. Khibnik and B. Krauskopf), World Scientific, 1998.
[6] A.D. Bazykin, F.S. Berezovskaya, G. Denisov and Y. A. Kuznetsov, *The influence of predator saturation effect and competition among predators on predator-prey system dynamics*, Ecol. Modelling, **14** (1981), 39–57.
[7] B. Boon and H. Landelout, *Kinetics of nitrite oxidation by nitrobacter winogradski*, Biochem. J., **85** (1962), 440–447.
[8] H.W. Broer, *Notes on Perturbation Theory*, in "Erasmus ICP Mathematics and Fundamental Applications", Aristotle University Thessaloniki, 1993.
[9] M.S. Boyce, C. Xu, *Dynamic complexities in a mutual interference hostparasitoid model*, Chaos, Solitons and Fractals, **24**(2005), 175–182.
[10] H.W. Broer, F. Dumortier, S.J van Strien and F. Takens, Structures in dynamics, finite dimensional deterministic studies, *Studies in Mathematical Physics 2*, North-Holland 1991; Russian translation, 2003. ISBN 0-444-89258-3.
[11] H.W. Broer, G.B. Huitema and M.B. Sevryuk, "Quasi-periodic Motions in Families of Dynamical Systems, Order Amidst Chaos," LNM 1645, Springer-Verlag, 1996.
[12] H.W. Broer, G.B. Huitema, F. Takens and B.L.J. Braaksma, *Unfoldings and bifurcations of quasi-periodic tori*, Mem. AMS (421), **83** (1990), 1–175.
[13] H.W. Broer and B. Krauskopf, *Chaos in periodically driven systems*, in "Fundamental Issues of Nonlinear Laser Dynamics" (ed. B. Krauskopf and D. Lenstra), American Institute of Physics Conference Proceedings 548 (2000), 31–53. ISBN 1-56396-977-7.
[14] H.W. Broer, V. Naudot and R. Roussarie, *Catastrophe theory in Dulac unfolding*, Preprint 2006.
[15] H.W. Broer, V. Naudot, R. Roussarie and K. Saleh, *A predator-prey model with non-monotonic response function*, to appear in Regular and Chaotic Dynamics, 2005.
[16] ———, *Bifurcations of a predator-prey model with non-monotonic response function*, C.R. Acad.Sci. Paris Ser. I, **341** (2005), 601–604.
[17] ———, *Proofs of the existence of bifurcations in a predator-prey system with non-monotonic response function*. Downloadable on http://www.math.rug.nl/∼broer/proof.pdf.
[18] H.W. Broer, V. Naudot, R. Roussarie, K. Saleh and F.O.O Wagener, *Organising centres in the semi-global analysis of dynamical systems*, to appear IJAMAS-Euler's volume 2005.

[19] H.W. Broer, C. Simó and J.C. Tatjer, *Towards global models near homoclinic tangencies of dissipative diffeomorphisms*, Nonlinearity, **11** (1998), 667–770.
[20] H.W. Broer, C. Simó and R. Vitolo, *Bifurcations and strange attractors in the Lorenz-84 climate model with seasonal forcing*, Nonlinearity, **15** (2002), 1205–1267.
[21] A. Chenciner, *Bifurcations de points fixes elliptiques. I. Courbes invariantes*, IHES–Publications mathématiques, **61** (1985), 67–127.
[22] ———, *Bifurcations de points fixes elliptiques. II. Orbites periodiques et ensembles de Cantor invariants*, Inventiones mathematicae, **80** (1985), 81–106.
[23] ———, *Bifurcations de points fixes elliptiques. III. Orbites periodiques de 'petites' périodes et élimination résonnante des couples de courbes invariantes*, IHES–Publications mathématiques, **66** (1988), 5–91.
[24] S.N. Chow and J.K. Hale, "Methods of Bifurcation Theory," Springer-Verlag, 1982.
[25] L. Díaz, J. Rocha and M. Viana, *Strange attractors in saddle cycles: prevalence and globality*, Inv. Math., **125** (1996), 37–74.
[26] D.M. Dubois, *Hyperincursive Simulation of Ecosystems Chaos and Patchiness by Diffusive Chaos*, International Journal of Computing Anticipatory Systems, **1** (1998), 51–68.
[27] E.J. Doedel, R.A. Champneys, T.F. Fairgrieve, Y.A. Kuznetsov, B. Sandstede and X.J. Wang, AUTO2000: Continuation and Bifurcation Software for Ordinary Differential Equations (with HomCont), User's Guide, Concordia University, Montreal, Canada 1997-2000. (http//indy.cs.concordia.ca).
[28] F. Dumortier, R. Roussarie and J. Sotomayor, *Generic 3-parameter families of vector fields on the plane, unfolding a singularity with nilpotent linear part. The cusp case of codimension 3*, Ergod. Th. & Dynam. Sys., **7** (1987), 375–413.
[29] F. Dumortier, R. Roussarie, J. Sotomayor and H. Zoladek, "Bifurcations of Planar Vector Fields," LNM 1480, Springer-Verlag 1991.
[30] S. Dunbar, *Travelling waves solutions of diffusive Lotka-Volterra equations: a heteroclinic connection in* $\mathbb{R}^4$, Trans. of AMS (2), **286** (1984), 557–594.
[31] V.H. Edwards, *Influence of high subtrate consentrations on microbial kinetics*, Biotechnol. Bioeng., **12** (1970), 679–712.
[32] H.I. Freedman and S. Ruan, *Hopf bifurcation in three-species food chain models with group defense*, Math. Biosci., **111** (1992), 73–87.
[33] H. I. Freedman and G. S. K. Wolkowicz, *Predator-prey systems with group defence: The paradox of enrichment revisited*, Bull. Math. Biol., **48** (1986), 493–508.
[34] G.F. Gause, *Experimental studies on the struggle for existence: I. Mixed population of two species of yeast*, J. Exp. Biol., **9** (1932), 389–390.
[35] C. Godbillon and Feuilletages, "Etudes Géométriques," Birkauser, 1991.
[36] W. Govaerts, Y.A. Kuznetsov and A. Dhooge, *Numerical continuation of bifurcations of limit cycles in MATLAB*, SIAM J. Sci. Comp., **27** (2005), 231–252.
[37] J. Guckenheimer and P. Holmes, "Nonlinear Oscillations, Dynamical Systems, and Bifurcations of Vector Fields," Springer-Verlag, 1990.
[38] D. Hanselman, "Mastering Matlab," University of Maine, 2001. (http://www.mathworks.com).
[39] C.S. Holling, *Some characteristics of simple types of predation and parasitm*, Can. Entomolog., **91** (1959), 385–398.
[40] B. Krauskopf, *Bifurcation sequences at 1:4 resonance: an inventory*, Nonlinearity, **7** (1994), 1073–1091.
[41] Y.A. Kuznetsov, "Elements of Applied Bifucations Theory," Springer-Verlag, 1995.
[42] A.J. Lotka, "Elements of Physical Biology," Williams and Wilkins, Baltimore MD, 1925.
[43] R.M. May, "Stability and complexity in model ecosystems," Princeton University Press, 1973.
[44] J.W. Milnor, "Topology from Differential Viewpoint," The University Press of Virginia, 1990.
[45] H. Malchow, F.M. Hilker and S.V. Petrovskii, *Noise and productivity dependence of spatiotemporal pattern formation in a prey-predator system*, Discrete and continuous Dynamical Systems, serie s B, **4** (2004), 705–711.
[46] L. Mora and M. Viana, *Abundance of strange attractors*, Acta Math., **171** (1993), 1–71.
[47] J.R. Munkres, "Elementary Differential Topology," Princeton Universtity Press, 1963.
[48] J. Palis and W. de Melo, "Geometric Theory of Dynamical System," Springer-Verlag, 1982.
[49] J. Palis and F. Takens, "Hyperbolicity and Sensitive Chaotic Dynamics at Homoclinic Bifurcations," Cambridge Studies in Advanced Mathematics 35, Combridge University press, 1993.

[50] V. Ray and W.M. Schaffer, *Chaos in Ecology*, Chaos, Solitons and Fractals, **12** (2001), 197–203.
[51] E. Renshaw, "Modelling Biological Populations in Space and Time," Cambridge University Press, 1991.
[52] S. Rinaldi, S. Muratori and Y.A. Kuznetsov, *Multiple attractors, catastrophes and chaos in seasonally perturbed predator-prey communities*, Bull. Math. Biol., **55** (1993), 15–35.
[53] R. Roussarie, *Bifurcations of Planar Vector Fields and Hilbert's Sixteenth Problem*, Progress in Mathematics 164, Birkhäuser, 1998.
[54] S. Ruan and D. Xiao, *Global analysis in a predator-prey system with nonmonotonic functional response*, SIAM J. Appl. Math., **61** (2001), 1445–1472.
[55] M. Scheffer, *Fish and nutrients interplay determines alga biomass: a minimal model*, OIKOS, **62** (1991), 271–282.
[56] K. Saleh, "Organising centres in the semi-global analysis of dynamical systems," Phd Thesis, University of Groningen, 2005.
[57] K. Saleh and F.O.O. Wagener, *Semi-global analysis of normal-internal k : 1 resonances*, Preprint 2005.
[58] E. Salomon, *The natural control of animal populations*, J. of Anim. and Eco., **18** (1949), 1–35.
[59] F. Takens, *Forced oscillations and bifurcations*, Applications of global analysis I Communications of the Mathematical Institute Rijksuniversiteit Utrecht 3 (1974), 1–59.
In "Global Analysis of Dynamical Systems, Festschrift dedicated to Floris Takens for his 60th birthday" (ed. H.W. Broer, B. Krauskopf, and G. Vegter), Institute of Physics, Bristol and Philadelphia (2001), 89–111.
[60] F. Takens, *Singularities of Vector Fields*, Publ. Math. IHES, **43** (1974), 47–100.
[61] F. Takens, *Unfoldings of certain singularities of vector fields. Generalized Hopf bifurcation*, Journ. Diff. Eqns., **14** (1973), 476–493.
[62] J.S. Tener, "Muskoxen," Queen's Printer, Ottawa, 1965.
[63] M. Viana, *Saddle-node critical cycles and prevalence of strange attractors*, course given at the University of Groningen.
[64] R. Vitolo, "Bifurcations of attractors in 3D diffeomorphisms: A study in experimental mathematics," PhD Thesis, University of Groningen, 2003.
[65] V. Volterra, *Variazioni e fluttuaziono del numero di individui in specie animali conviventi*, Mem. Accad. Lincei., **2** (1926), 31–113.
[66] S. Wolfram, "The Mathematica book," Cambridge University Press, Wolfram research Inc. 1996. (http://www.wolfram.com).
[67] D. Xiao and S. Ruan, *Codimension two bifurcation in a predator-prey system with group defense*, Int. J. bif. & chaos, **11** (2001), 2123–2131.
[68] H. Zhu, S. A. Campbell, and G.S.K. Wolkowicz, *Bifurcation analysis of a predator-prey system with nonmonotonic functional response*, Siam J. Appl. Math., **63** (2002), 636–682.

Received March 2006; revised January 2007.

E-mail address: h.w.broer@rug.nl
E-mail address: khairul@math.rug.nl
E-mail address: vijnc@maths.warwick.ac.uk
E-mail address: roussari@u-bourgogne.fr